



Title	Identifying damage in a bridge by analysing rotation response to a moving load
Authors(s)	Hester, David, Brownjohn, J. M. W., Huseynov, Farhad, O'Brien, Eugene J., González, Arturo, Casero, Miguel
Publication date	2019-11-04
Publication information	Hester, David, J. M. W. Brownjohn, Farhad Huseynov, Eugene J. O'Brien, Arturo González, and Miguel Casero. "Identifying Damage in a Bridge by Analysing Rotation Response to a Moving Load." Taylor & Francis, November 4, 2019. https://doi.org/10.1080/15732479.2019.1680710 .
Publisher	Taylor & Francis
Item record/more information	http://hdl.handle.net/10197/11493
Publisher's statement	This is an Accepted Manuscript of an article published by Taylor & Francis in Structural and Infrastructure Engineering on 4 November 2019, available online: http://www.tandfonline.com/10.1080/15732479.2019.1680710
Publisher's version (DOI)	10.1080/15732479.2019.1680710

Downloaded 2026-04-30 22:38:57

The UCD community has made this article openly available. Please share how this access benefits you. Your story matters! (@ucd_oa)



© Some rights reserved. For more information

Identifying damage in a bridge by analysing rotation response to a moving load

David Hester¹, James Brownjohn², Farhad Huseynov^{3, 4}, Eugene OBrien³, Arturo Gonzalez³, Miguel Casero Florez³

¹ School of Natural and Built Environment, Queen's University Belfast, Stranmillis Road, BT9 5AG Belfast, Northern Ireland, UK.

² Vibration Engineering Section, College of Engineering, Mathematics and Physical Sciences, University of Exeter, North Park Road, EX4 4QF Exeter, UK

³ School of Civil Engineering, University College Dublin, Newstead, Belfield, Dublin, D04 V1W8, Ireland

⁴ Full Scale Dynamics LTD, Kay Building North Park Road, Exeter EX4 4QF

Contact author: Farhad Huseynov

Kay Building North Park Road,

Exeter. UK

EX4 6BH

E-mail: f.huseynov@fullscaledynamics.com

Tel: 07533118686

Body text word count:

Number of figures:

Number of tables:

Abstract

This paper proposes a bridge damage detection method using direct rotation measurements. Initially, numerical analyses are carried out on a 1-D simply supported beam model loaded with a single moving point load to investigate the sensitivity of rotation as a main parameter for damage identification. As a result of this study, the difference in rotation measurements due to a single moving point load obtained for healthy and damaged states is proposed as a damage indicator. A relatively simple laboratory experiment is conducted on a 3 m long simply supported beam structure to validate the results obtained from the numerical analysis. The case of multi-axle vehicles is investigated through numerical analyses of a 1-D bridge model and a theoretical basis for damage detection is presented. Finally, a sophisticated 3-D dynamic Finite Element model of a 20 m long simply supported bridge structure is developed by an independent team of researchers and used to test the robustness of the proposed damage detection methodology in a series of blind tests. Rotations from an extensive range of damage scenarios were provided to the main team who applied their methods without prior knowledge of the extent or location of the damage. Results from the blind test simulations demonstrate that the proposed methodology provides a reasonable indication of the bridge condition for all test scenarios.

Keywords: Bridge, damage detection, rotation, inclinometers, influence line, SHM, BHM.

1 Introduction

As bridges deteriorate over time and due to accidental damage, owners and managers seek to estimate their remaining safe working life. Structural Health Monitoring (SHM) has the potential to be a key input into this process, providing as it does, an indication of the bridge's current health state (Heitner et al 2019). This paper proposes the use of bridge rotation response to a moving load for SHM purposes, to indicate the presence of damage and its location in a bridge. In this study, damage is represented as a reduction in the Second Moment of Area of a bridge deck over a certain extent along its length. Like vertical translation due to a moving force, rotation responds to local damage anywhere in the bridge, but rotation is typically easier to measure than translation. To give context to this work, Section 1.1 gives a brief overview of bridge SHM approaches, Section 1.2 reviews studies where inclinometers have been installed on bridges previously and Section 1.3 describes the objectives of this study.

1.1 Existing approaches to damage identification in a bridge subject to a moving force

Some authors use a wavelet transform of beam translation (W. W. Zhang, Wang, & Ma, 2009; Zhu & Law, 2006) or acceleration (Hester & González, 2012) response to a moving vehicle to locate damage in a beam, while other researchers have applied empirical mode decomposition to the acceleration response (Bradley, González, & Hester, 2010; N. E. Huang, Huang, & Chiang, 2005). O'Brien, Carey and Keenahan (2015) use an indirect approach; they apply a Moving Force Identification algorithm to the translation response and use the calculated force histories as indicators of bridge damage. In another indirect approach, Li and Au (2014) calculate the modal strain energy of the acceleration signals from multiple vehicle passes and succeed in localising damage from the extracted frequencies of healthy and damaged bridges. Others use

strain response in a bridge to ambient traffic and identify damage from a change in the position of the neutral axis of the main girders (Park, Moon, Spencer, & Sim, 2017; Sigurdardottir & Glisic, 2013, 2014, 2015) or a change in the transverse load distribution factors (Cardini & DeWolf, 2009).

1.2 Rotation measurement in bridges

Inclination sensors (inclinometers or tiltmeters) are designed to measure angular rotation of a test specimen with respect to an ‘artificial horizon’. The main operating principle of most inclinometers is that they perform measurements of different types of response generated by pendulum behaviour due to gravity. The types of pendulum used in inclinometer sensors can be categorized as solid mass (Chang, Tsai, Liu, Sun, & Fang, 2011), liquid (Liu & Zhu, 2017) and gas (Crescini, Marioli, Romani, Sardini, & Taroni, 2004; F. Zhang, 2004), and these are measured using resistive (W. Zhang, Zhu, & Lee, 2015), capacitive (Zhao & Yeatman, 2007), inductive (Olaru & Dragoi, 2005), magnetic (Olaru & Cotae, 1997), fibre optic (Antunes, Marques, Varum, & Andre, 2012) or optical (Frazão et al., 2006) methods. In the last decade, the performance and accuracy of inclinometers have been significantly improved, and it is now possible to measure inclinations to a microradian (10^{-6} rad) accuracy using state-of-the-art sensors (Bruns, 2017; Inaudi & Glisic, 2002; Wu & Chuang, 2004; Wyler AG, 2016).

Inclinometers have been widely utilized in industrial applications such as automotive, aerospace and electronics. With recent improvements in sensor technology, they have also been used in bridge SHM applications. Haritos and Chalko (1996) installed inclinometers at the support locations of Fuge’s Bridge to obtain a better understanding of its boundary conditions. They concluded that the behaviour of bearings at the abutments corresponds more closely to “pinned” than “fixed”, for which

the bridge was originally designed. In a similar study, Micro-Electro-Mechanical Systems (MEMS) inclinometers were installed on Ferriby Bridge in the UK to investigate the long-term transverse inclination of elastomeric bearing due to temperature effects (Hoult, Fidler, Hill, & Middleton, 2010; Stajano et al., 2010). Shoukry, Riad, and William (2009) instrumented a steel bridge built according to the AASHTO LRFD bridge design specification (American Association of State Highway and Transportation Officials, 2012), to evaluate the long-term performance of the bridge deck and compare the measured bridge response with the theoretical approaches proposed in the LRFD code.

Glišić, Posenato, Inaudi, and Figini (2008) monitored a curved concrete bridge during its construction, post-tensioning and first year of service life using fibre optic interferometric technology including long-gauge deformation sensors and inclinometers. The results obtained from the campaign helped to verify post-tensioning and confirmed the sound performance of the bridge. Others installed inclinometers on long-span suspension and cable stayed bridges in an effort to better understand the behaviour of such complex structures (Andersen, Enckell, Alcover, & Chryssanthopoulos, 2013; Bas, Apaydin, Ilki, & Catbas, 2018; Ko & Ni, 2005; H. Li & Ou, 2016). Inclinometers have also been used to calculate the deformed shape of bridge deck structures (Burdet & Zanella, 2000; He, Yang, & Zhao, 2014; Helmi, Taylor, Zarafshan, & Ansari, 2015; Hou, Yang, & Huang, 2005; LLoret, Inaudi, & Vurpillot, 1998; O'Leary & Harker, 2012; Perregaux, Vurpillot, Inaudi, & Burdet, 1998; Robert-Nicoud, Raphael, Burdet, & Smith, 2005; Sousa, Cavadas, Henriques, Bento, & Figueiras, 2013; Vurpillot, Krueger, Benouaich, Clément, & Inaudi, 1998), the advantage being that unlike any other direct methods of measuring bridge deflections, inclinometers do not require a reference point.

Alten, Ralbovsky, Vorwagner, Topplitzer, and Wittmann (2017) evaluated different monitoring techniques through a progressive damage case study conducted on a post-tensioned reinforced concrete bridge over a 12 week period. The test bridge was instrumented with 23 sensors: 6 accelerometers, 2 biaxial inclinometers (at support locations) and 15 fibre-optic strain gauges. Three different damage scenarios were considered for the bridge within the scope of the study and bridge evaluation using the inclinometers was found to be the most effective. An increase in magnitude of rotation was clearly observed in both channels as a result of the damage imposed, while the accelerometers (used to monitor changes in modal frequencies) failed to identify all three damage scenarios. Of the 16 strain sensors, only those close to the damage locations recorded an increase in strain and these increases were small.

Although it has been demonstrated in several recent studies that inclinometers could be valuable in assessing the condition of bridge structure, there are a limited number of studies in the literature that use direct rotation measurements for the assessment of the condition of a bridge. The only bridge damage detection methodologies that the authors found in the literature are recent studies presented by Erdenebat, Waldmann, Scherbaum and Teferle (2018) and Zeinali and Story (2017, 2018). Erdenebat et al. (2018) propose a method named Deformation Area Difference (DAD) for the condition assessment of bridge structures which identifies damage using the area between the rotation curves measured for healthy and damaged bridge conditions under static loading. It is demonstrated in the study through numerical and experimental studies that the maximum amplitude of the DAD factor occurs at the location where the damage occurs. The developed methodology could be applied through rotation, vertical deflection or curvature measurements. However, the drawback

of the proposal is that it requires deformation measurements at many locations along the length of the structure, which makes bridge closures likely.

Zeinali et al. (2017, 2018) present a novel theoretical framework for estimating the flexural stiffness of a bridge deck using its deflection or rotation responses to a moving load. It is demonstrated through numerical and relatively simple experimental studies that the stiffness of the entire bridge span can be estimated. This is achieved using the relationship between the second derivative of the deformation (i.e. deflection or rotation) influence line for a single measurement location and the flexural rigidity. Once the flexural stiffness distribution of a bridge is calculated, then damage can be identified as a change in this distribution. Although the proposed methodology is promising in identifying damage on real bridges, both numerical and experimental studies are carried out using single moving point analysis. Besides, the magnitude of rotation measurements presented in the experimental study is around 5 degrees, much greater than the amplitude of rotations expected in a real bridge.

1.3 Objective of this study

Although the field of SHM has witnessed significant advances over the last two decades, identifying small levels of damage in a bridge still remains a challenge. Broadly speaking existing SHM systems, some of which are reviewed above, mainly use acceleration, strain and/or deflection responses of a bridge to evaluate its condition. Each parameter has certain shortcomings. Acceleration, despite of its popularity, is relatively insensitive to damage except the most onerous damage scenarios. Strain sensors measure a local response of a bridge hence they can only sense damage at the immediate vicinity. Deflections, although being damage sensitive, are often difficult to

measure in practice due to nature of its parameter (e.g. a reference point for measurements may be required).

There is a lack of study in literature using rotation measurements for bridge condition assessment. The available studies mainly monitor changes in the amplitude of rotation measurements, neglecting the variability in the responses that naturally arise from the variability in the random traffic loads (i.e. vehicle weight and configuration). Such techniques have been shown to be effective in only suggesting the existence of damage in a bridge without giving knowledge of its location. Among the existing studies only a few rotation based damage detection methodologies look at identifying the location of anomaly in a bridge however such techniques require a bridge to be installed with a vast number of sensors (Erdenebat et al., 2018).

To address the limitations of existing studies described in the literature, this study presents novel contributions in 3 specific areas;

- A new bridge condition assessment methodology is proposed that uses direct rotation measurements for damage identification. Like deflections, rotations are damage sensitive anywhere on the bridge but they easier to measure compared to deflections using the state-of-the-art sensors.
- The influence line of a bridge to a moving load is derived from each rotation response to a traversing vehicle to provide a “normalised” response that can be compared for all measurements, regardless of the vehicle that induced it.
- The proposed methodology can identify the existence of damage and its location with a reasonable accuracy using data from two sensors installed at the bridge supports, at the deck level. A sparse number of sensors

provide a cost effective and less computationally expensive solution than existing approaches.

In the context of this study, Section 2 investigates the potential of direct rotation measurements in assessing the condition of bridge type structures and introduces the concept of identifying damage in the rotation signal for a beam subject to a moving point force. Numerical and experimental demonstrations of the concept are provided in Sections 2.1 and 2.2 respectively. Section 3 looks at the more challenging problem of identifying damage when the bridge is loaded by a multi-axle vehicle and further validates the robustness of the methodology through blind test simulations conducted on a 3-D FE model of a typical 20m long simply supported bridge.

2 Damage detection in a beam using rotation measurements due to a moving point load

This section develops the theoretical basis for the proposed damage detection method using rotation measurements when a beam is loaded with a single moving point force. Section 2.1 investigates the sensitivity of rotation to detect damage in bridge type structures through numerical analysis, and Section 2.2 presents the results obtained from an experimental study to validate the feasibility of the proposed method.

2.1 Sensitivity of rotation to damage

In theory, the change in rotation between any two points along the length of the structure is equal to the area under the M/EI diagram, where M is moment and EI is stiffness. Hence, in principle, any change in a structure's stiffness, either locally or globally, should be evident in the rotation measurements of the structure. To demonstrate this, numerical simulations are carried on a 1-D simply supported

numerical beam model loaded with single point force to address the following questions:

- Is rotation a sensitive parameter to damage?
- What is the effect of change in stiffness and its location on rotation measurements?
- What is the optimum sensor location for recording rotations?

The structure modelled is a 3m long 1-D simply supported beam structure. The flexural properties adopted for the beam are similar to those of a 127×76×13 universal beam loaded in the weak direction (Steel Construction Institute, 2015). The Young's modulus is defined as 210 GPa and the hypothetical sensors (inclinometers) are placed at three locations, i.e. at mid-span and the two support locations. Figures 1 (a) and (b) show the elevation and cross-section of the numerical beam model.

[insert Figure 1.]

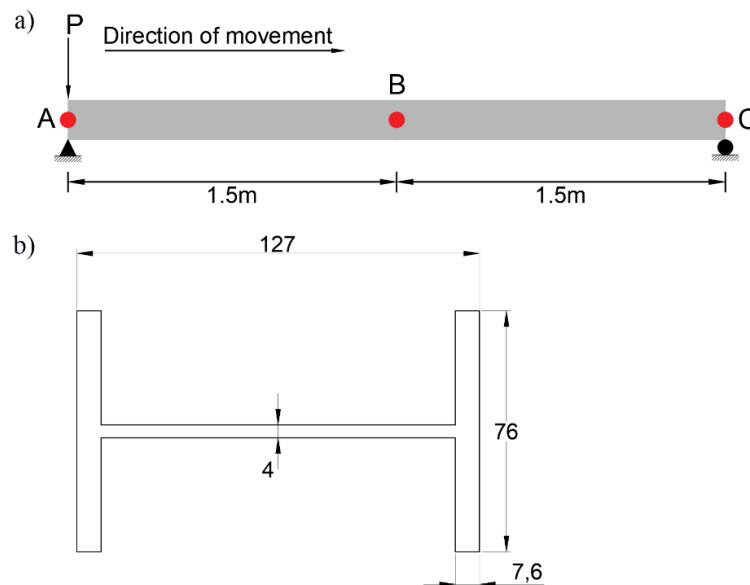


Figure 1. Numerical beam model a) Elevational view showing sensor locations b) Cross-sectional view.

In this section three damage scenarios are investigated, at quarter-span, at the centre, and at two simultaneous locations (i.e. at quarter- and three-quarter-span). For all scenarios investigated in this section, damage is modelled as a 30% reduction in Second Moment of Area for an extent of 180 mm (6% of the beam span), and the effect of damage on the bridge response is examined under a 31 kg point loading. Figure 2(a) presents the deformed shape of the first damaged beam model loaded with the 31 kg load at $3L/8$ and damage at quarter-span. The continuous curve represents the translation of the healthy beam while the dashed red curve shows the corresponding results for the damaged beam. As expected, when damage occurs, translation increases. Assuming that baseline (healthy) data will be available, the difference in translation between the healthy and damaged beam cases is plotted in Figure 2(b). The shape of the difference plot is triangular, with the maximum corresponding to the damage location. Rotation is the first derivative of translation and, with this sign convention, varies from negative before the damage location to positive after it – Figure 2(c). As translation difference (healthy minus damaged) varies from constantly sloping down to constantly sloping up, rotation difference varies from constant negative to constant positive, with a sharp change at the damage location – Figure 2(d). In fact, at the centre of the damaged location the difference in rotation between the healthy and damaged case is close to zero. This simply shows that the sensitivity of a sensor to damage reduces when sensor is at the damage location.

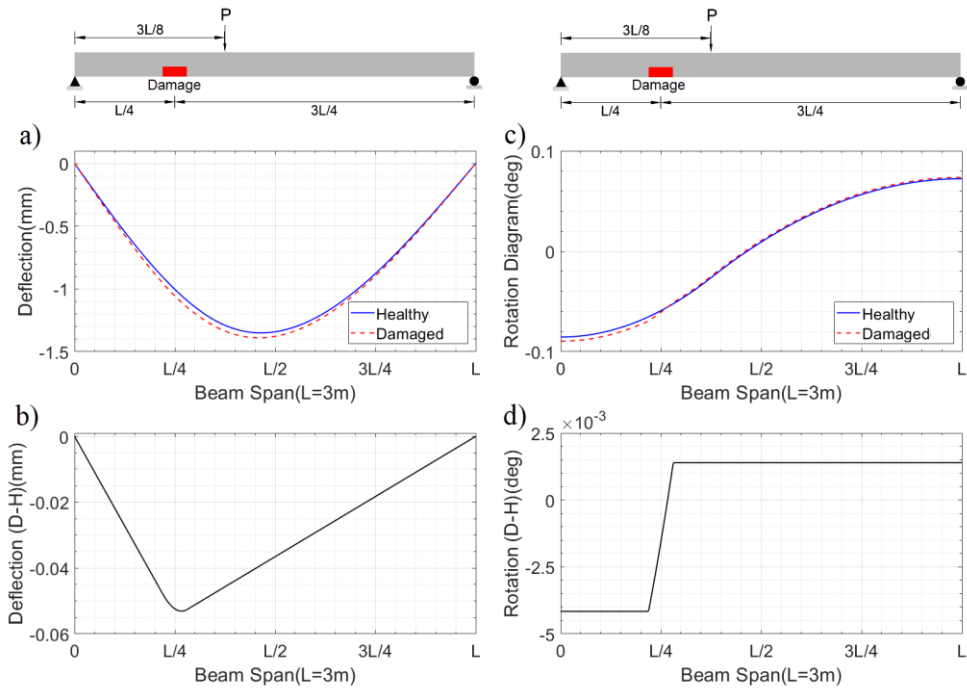


Figure 2. Displacement responses of healthy and damaged beam models loaded with a single point load at $3L/8$. a) Translation b) Difference in translation between healthy and damaged cases c) Rotation d) Difference in rotation between healthy and damaged cases.

A further consequence of the plot in Figure 2(d) is that for the single load location and the damage scenario represented here, the sensor at mid-span and the sensor at the right support will show the same difference in rotation. The amplitude of the rotation difference is greater on the left-hand side of the damage than on the right. It simply means that sensors placed along the beam length from the damage location to the closest support location are more sensitive to damage than the sensors placed on the opposite side.

The plots in Figure 2 are in the spatial domain, i.e. the displacements at all points on the beam are plotted for a fixed point in time and therefore a fixed position of the

load. In reality having sensors everywhere on the beam is not feasible but it will be shown that the concepts illustrated in Figure 2 are still relevant in the time domain for a moving point loading crossing a beam. Figure 3 (a) presents the rotation response obtained at sensor locations A-C under a 31 kg moving point loading for healthy and off-centre damaged case (i.e. damage is at $L/4$ location). In this case, rotation is plotted against the location of the moving point force. Sensors A and C, placed at the support locations, experience negative and positive rotation, respectively, as the point load crosses the beam. The Sensor B at mid-span initially experiences positive rotation but this becomes negative when the load passes this point. For sensor A, the increase in rotation due to damage is small but clearly evident. For sensors B and C the increase in rotation due to damage is smaller. Overall the figure shows that when damage occurs, even if it is remote from the sensor location, it results in an increase in rotation at all three sensor locations and confirms that, as expected, rotation increases when stiffness is reduced.

The differences between the rotation responses for healthy and damaged beam cases, are plotted in Figure 3(b). The rotation difference for each sensor is triangular with maximum amplitude when the load is over the damage location (at $L/4$ in this case). The magnitude of the rotation difference, which reflects the sensitivity of a particular sensor to damage, is approximately 4.8 mdeg for Sensor A, located at the left-hand support and 1.5 mdeg for Sensors B and C, located at mid-span and the right-hand support. These results are similar to the findings presented in Figure 2. Since Sensor A is located at the support closer to the damage location, it is more sensitive to damage than Sensors B and C. Also note that Sensors B and C are both on the same side of the damage location (to the right in this case) and hence have the same sensitivity to

damage. The reason that sensors B and C are showing the same sensitivity to damage can be understood by examining Figure 2(d).

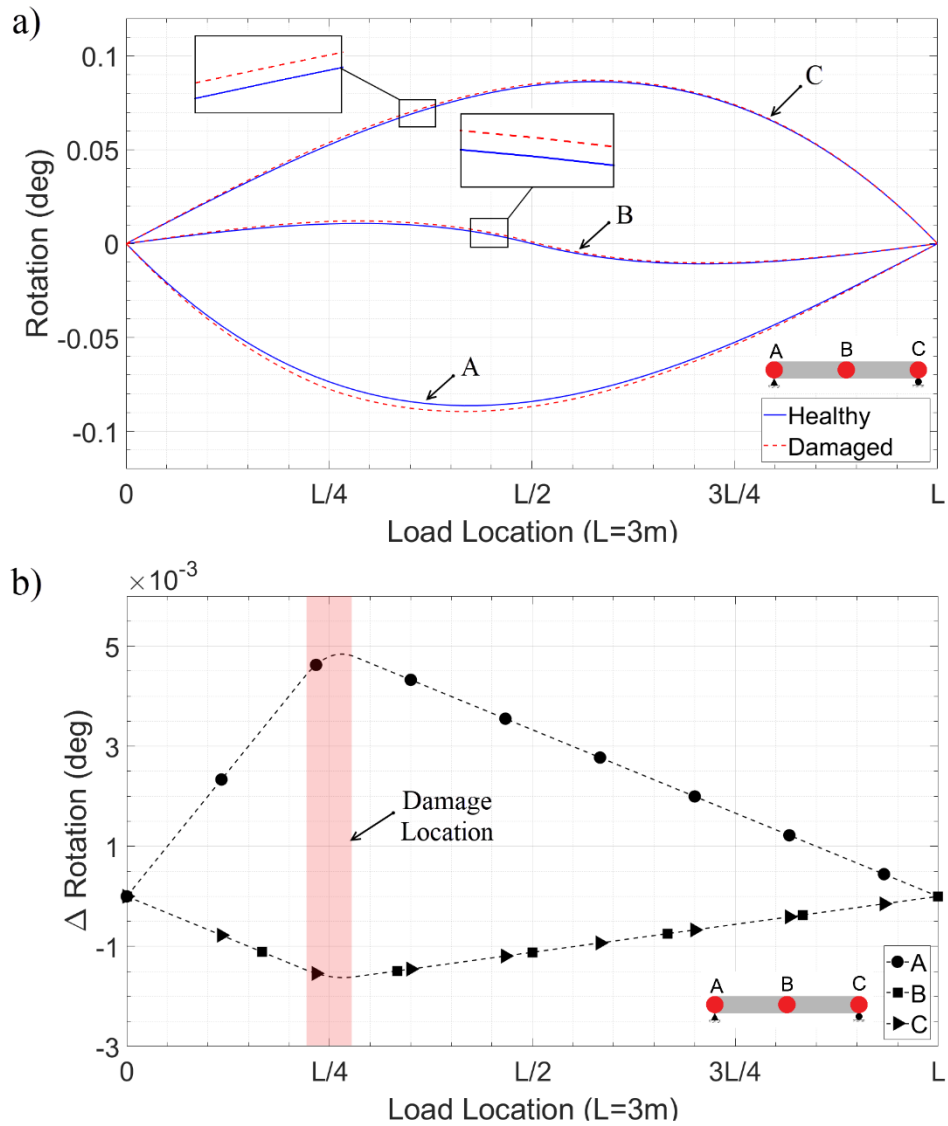


Figure 3. Effect of quarter-point damage on beam rotation measurements (a) Rotation time history recorded for healthy and damaged beam cases. (b) Differences between the healthy and damaged rotation signals shown in part (a).

Figure 4 shows the rotation difference when damage is simulated at midspan. For Sensors A and C placed at the supports the differences are triangular with a peak value of 4.25 mdeg and the peak corresponding to the damage location. However, for Sensor B at midspan the amplitude of the difference in rotation is much smaller and it is not triangular in shape. This is because, Sensor B is located at the damage location, where the change in rotation due to damage is close to zero which is consistent with the behaviour previously observed in Figure 2(d).

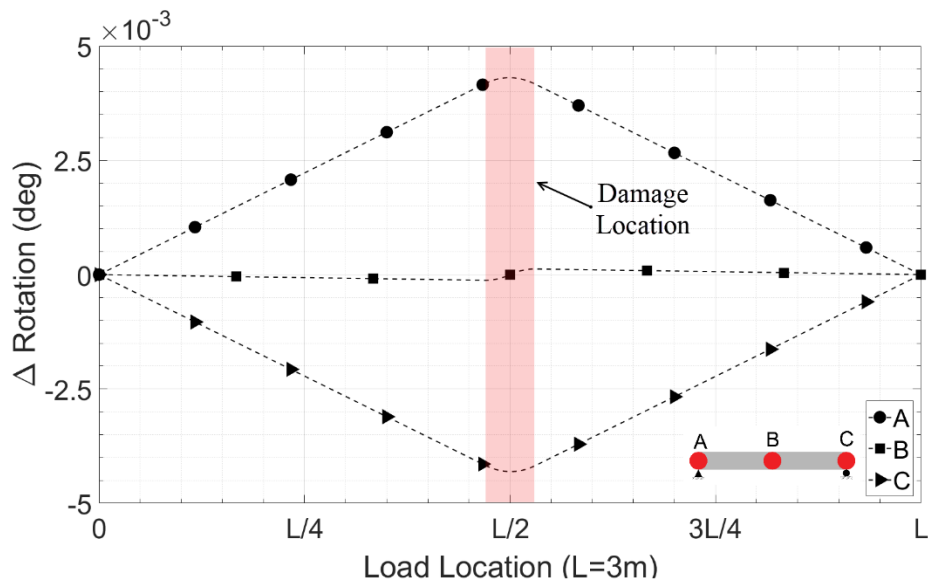


Figure 4. Difference in rotation measurements for healthy and damaged beams where damage is at midspan.

Figure 5 shows the rotation difference plot for a multiple damage scenario, where damage is modelled similarly at the quarter and three-quarter span locations. The damage severity for both locations is a 30% reduction in stiffness over 180 mm. It is clearly visible in the figure that there are two slope discontinuities can be seen in each plot, corresponding to the passing of the load over the damage locations. The rotation

difference amplitudes are approximately 5.5 mdeg and 3.25 mdeg at the damage locations for Sensors A and C. The corresponding results for Sensor B, located at midspan, are approximately 1 mdeg and vary in sign.

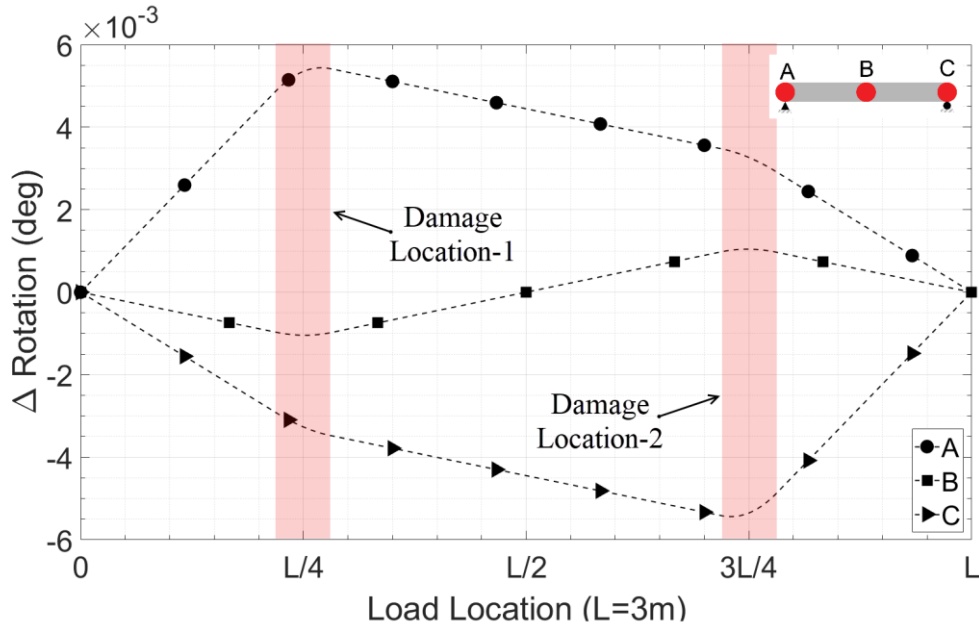


Figure 5. Difference in rotation measurements between healthy and damaged beam cases where damage is modelled at $L/4$ and $3L/4$.

In conclusion, when damage occurs in a bridge structure, it is evident in rotation measurements. Furthermore, the differences between rotations plots for healthy and damaged beam cases provide information on the damage locations. Sensitivity tends to be better for sensors placed in the zone between the damage and the nearest support to the damage. However, there is a reduced magnitude of rotations for sensors close to the centre of the damage. Support locations are chosen here as a good compromise for short span bridges with the further advantage that access on site is likely to be easier.

2.2 Experimental Validation

An experimental study was carried out on a 3 m long simply supported beam to validate the results of the simulations presented in Figure 4. Section 2.2.1 describes the laboratory setup and instrumentation used, while Section 2.2.2 presents the results.

2.2.1 Laboratory Setup

The material and geometric properties of the beam structure was designed to be similar to the flexural properties defined for the 1-D beam model used in the numerical studies presented above. The beam was a 127x76x13 steel universal beam loaded in the weak direction. The supports of the beam were fabricated to function as pin and roller. A 31 kg dumb-bell mass was used to load the structure at discrete points. The load was applied in a series of static load cases at 100 mm intervals along the length of the beam. At each loading position the load remained stationary for approximately 45 s before it was rolled to the next loading position.

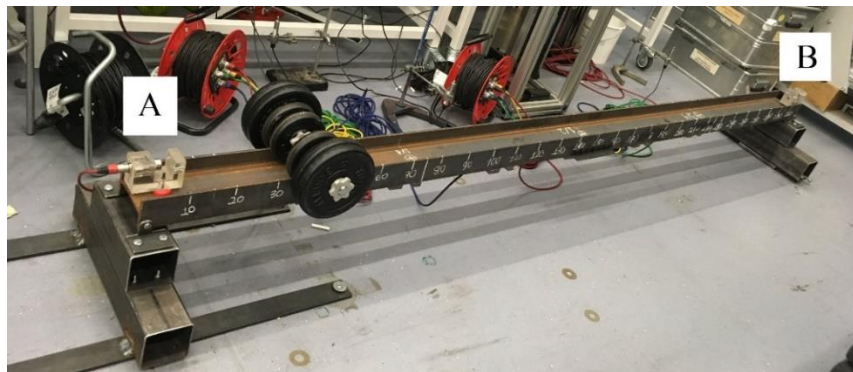


Figure 6. 3 m long simply supported beam structure set up in the laboratory with load at 0.4 m and rotation sensors at supports.

Rotations were calculated using the acceleration data obtained from two uniaxial Honeywell QA-750 accelerometers placed at the ends of the beam and orientated in the longitudinal direction (i.e. at points A and B in Figure 6). These accelerometers can sense frequencies as low as 0 Hz, so they can sense gravity and are suitable to be used as inclinometers. Data acquisition was carried out at a 512 Hz sampling rate using a 24-bit Data Physics Mobiliser II spectrum analyser, controlled by a computer.

The output of an accelerometer follows a sinusoidal relationship when it is rotated through gravity (g). When it is oriented in the horizontal direction it records 0 g whereas when it is placed in the vertical direction it reads ± 1 g. From basic trigonometry, the rotation is obtained from acceleration, Acc , using the inverse sine function given in Eq.1:

$$\theta = \sin^{-1}(Acc[g]) \quad (1)$$

As the 31 kg mass is moved in 100 mm increments across the bridge, it is not possible to apply it perfectly 'statically' at each location, (i.e. it is not applied infinitely slowly). As a result, some dynamic movements of the beam occur in the immediate aftermath of placing the load.

Figure 7(a) shows the raw acceleration time history data from the accelerometer placed at point A as the mass is moved across the length. At each loading position, the mass remained stationary for approximately 45 s. There are 29 peaks in the figure corresponding to 29 loading positions (0.1 to 2.9 m in intervals of 0.1 m). A low pass filter is applied to remove the high frequency content of the response. This high frequency content is due to the dynamic movements which inevitably occur when the load is not applied perfectly statically. Subsequently rotation is calculated using Eq. 1. Figure 7(b) shows the rotation calculated from the accelerometer placed at point A.

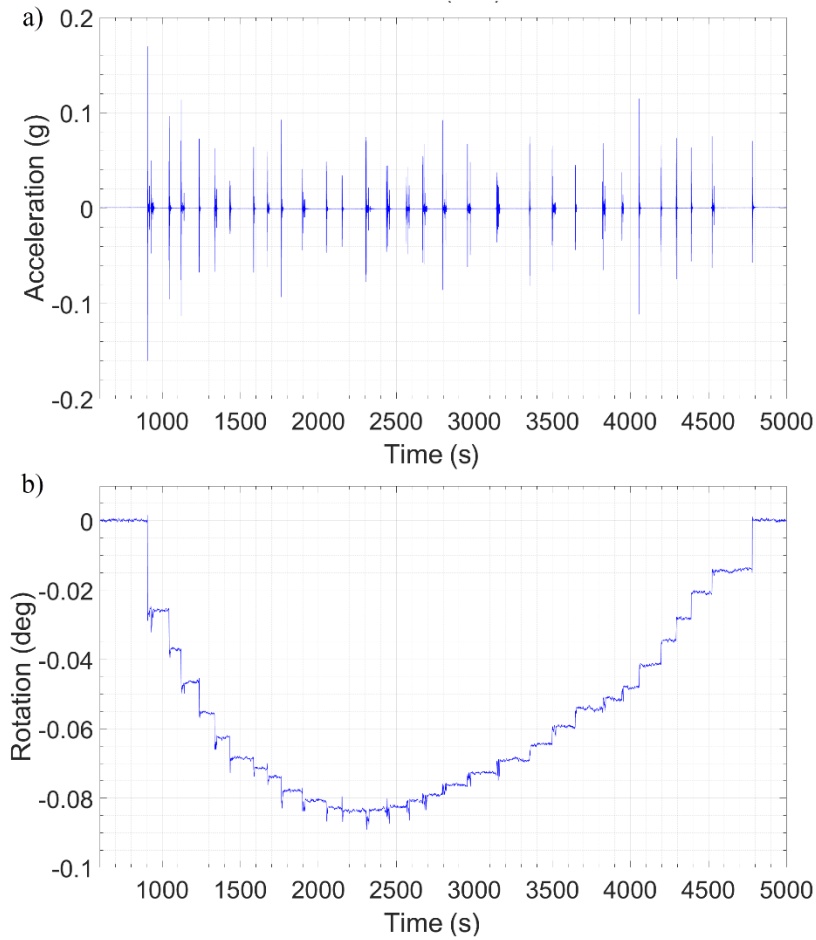


Figure 7. Experimental results for accelerometer at the left-hand support while it is statically loaded with a 31 kg dumbbell. (a) Acceleration time history (b) Rotation time history calculated from the measured accelerations.

To show that the levels of rotation of Figure 7(b) are representative of the levels experienced in a real bridge, Figure 8 shows the results of a load test performed on a 17.8 m span bascule bridge, loaded with a 4-axle 32 tonne truck. When the bridge is down it behaves as a simply supported bridge. The accelerometers used in the bridge to calculate rotations at the support locations are the same QA-750s used in the laboratory

test. Overall, the maximum amplitudes of rotations recorded during the field testing and the laboratory experimentation are similar being 1.1 deg and 0.08 deg, respectively.

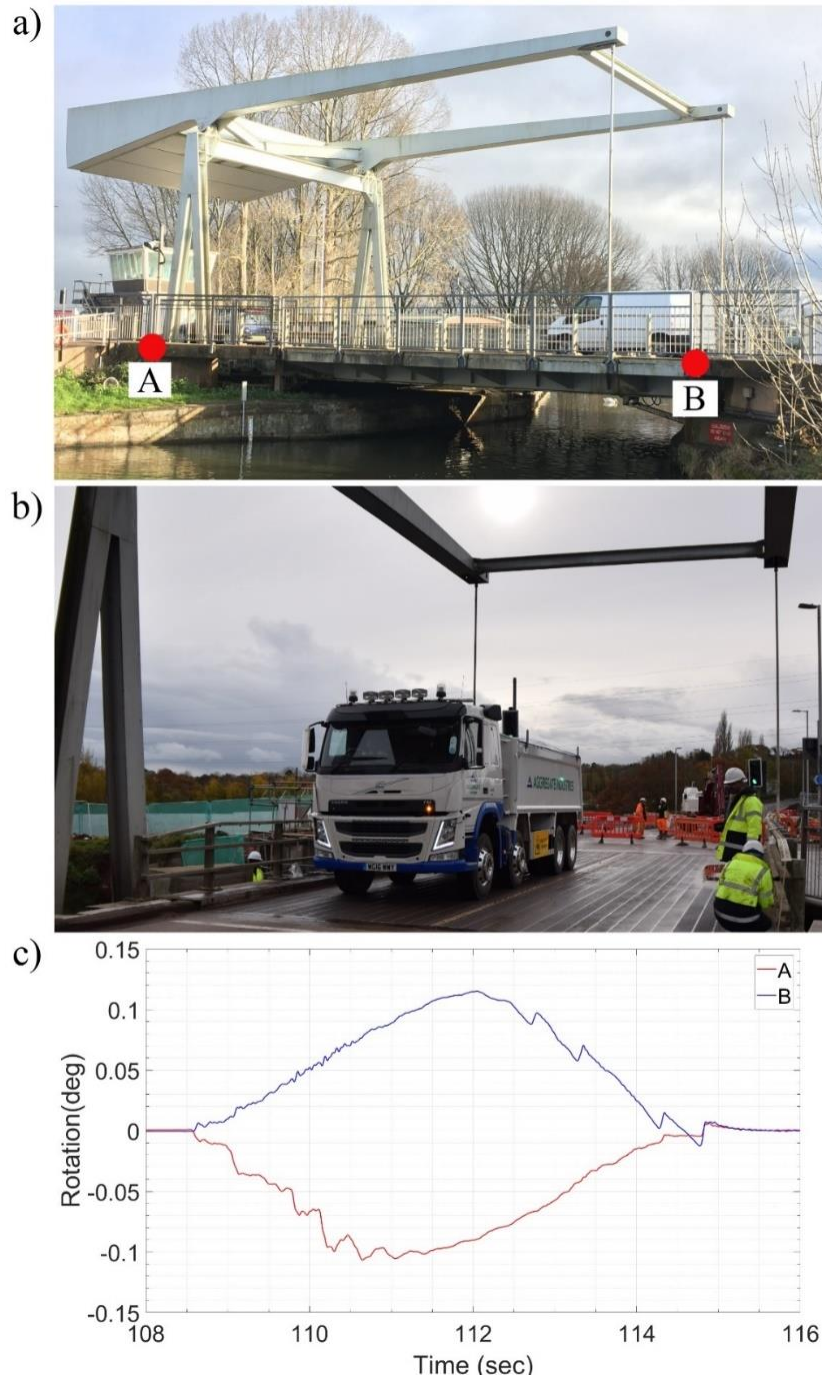


Figure 8. Recording rotations on a real bridge, a) Elevation of the test structure b) 4-axle 32 tonne test truck c) Rotation time history calculated at support locations.

2.2.2 Rotation measurements in stiffened laboratory beam

The simply supported beam structure in the laboratory was initially loaded using the 31 kg point load at 29 locations. This is assumed to be the healthy beam case. Subsequently, the beam was stiffened at the midspan location using steel angle sections to simulate negative damage. The negative damage concept is non-destructive and allows the beam to be used for other purposes after the test. To test repeatability, the healthy and stiffened beams were both loaded four times. The steel angle sections were 180 mm long and increased the second moment of area of the cross section by 33%.

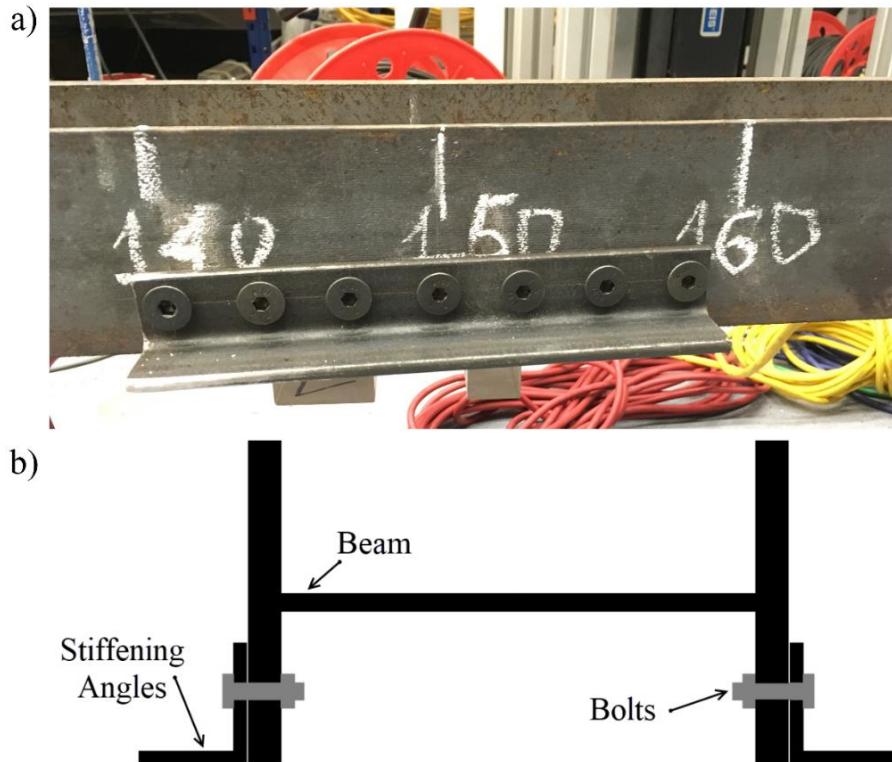


Figure 9. Beam stiffening detail (a) Elevation view of the stiffening angles. (b) Cross section of beam and stiffeners.

Figure 10(a) shows the rotations measured at the left end (sensor A) and right end (sensor B) for all load positions. In total there are four plots for the original beam and four for the stiffened beam cases for each accelerometer (see insert in the figure). The figure shows that the two measurements are consistent (hence reliable) and that the rotations for the stiffened beam are less than for the original (healthy) beam. The average of the four rotation measurements calculated for the original beam case is subtracted from the corresponding average rotation for the stiffened beam cases and the results for sensor locations A and B are presented in Figures 10 (b) and (c) respectively. Each point in the plots represents the rotation difference for a given loading position. The red line plots in Figures 10 (b) and (c) show the numerically predicted difference in rotation calculated using the numerical model discussed in Section 2.1. It can be seen that the experimentally measured points agree well with the predictions and the plots approximate a triangular shape with the peak corresponding to the stiffening location. It can be concluded that stiffening at this level can be successfully detected in a laboratory setting.

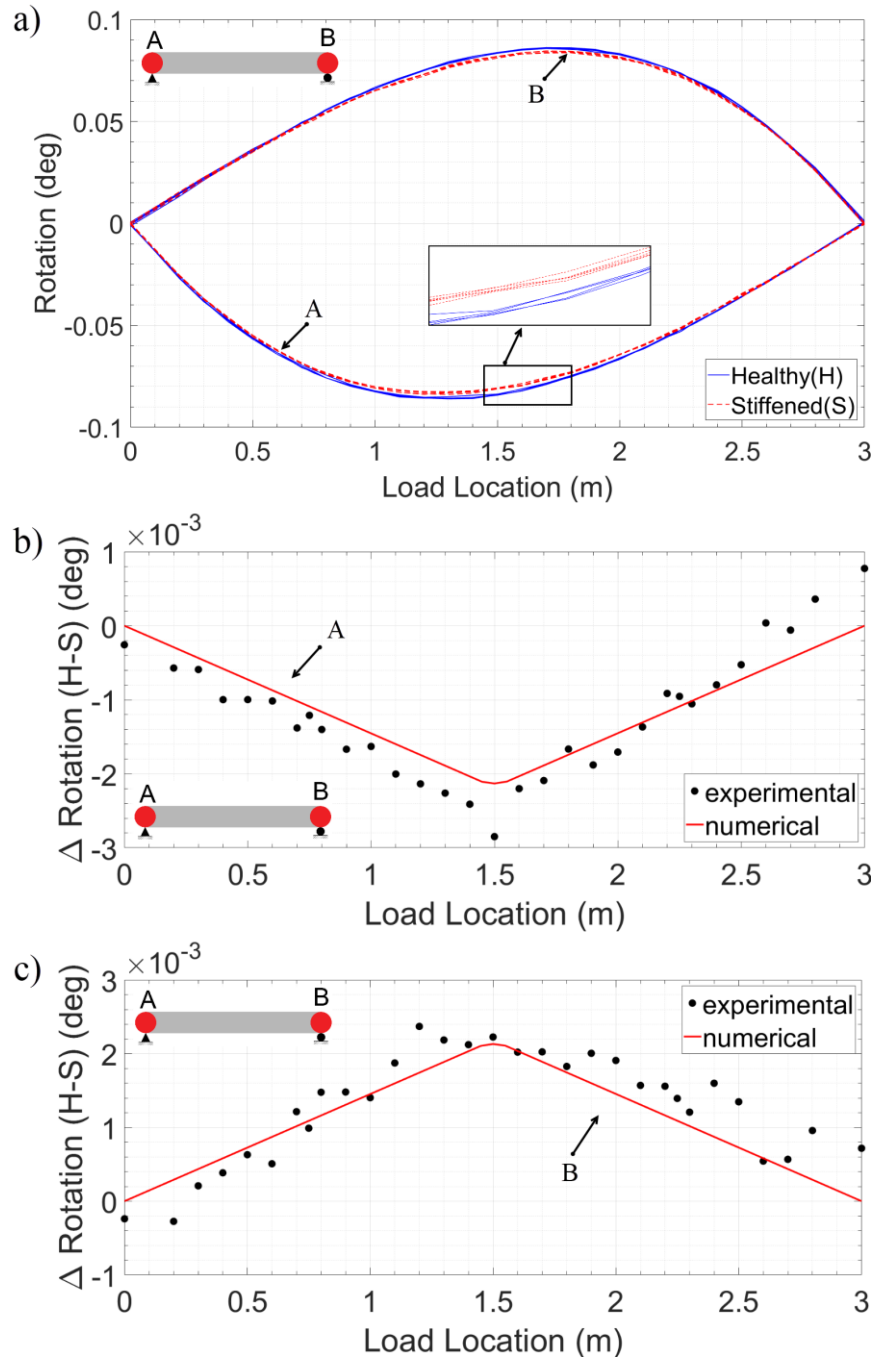


Figure 10. Effect of damage on beam rotation measurements (a) Rotation versus load location (b) Difference in rotation measurements for healthy and stiffened beam cases for sensor at the left-hand support (Point A) (c) Difference in rotation measurements for healthy and stiffened beam for sensor at the right-hand support (Point B).

3 Damage detection for a multi axle vehicle

This section investigates the damage detection method when the rotation response is due to a multi-axle vehicle. Initially, a static 1-D bridge model is used to develop the theoretical basis of the proposed damage detection method. Subsequently, a 3-D bridge model is used to simulate dynamic vehicle-bridge interaction and to test the robustness of the proposed bridge damage detection method on more realistic bridge signals.

3.1 Theoretical basis for multi-axle vehicle

In this section simple static analyses are carried out on a 1-D bridge model to investigate the application of the proposed damage detection method to a multi-axle vehicle signal. The bridge is modelled as a 20 m long simply supported beam. The flexural properties adopted are typical for a 10 m wide bridge structure consisting of 9 No Y3 precast beams spaced at 1.25 m centres with a 160 mm thick deck slab (“Concast Precast Group Concrete Prestressed Girders Technical Guide” 2009). This results in a total depth of 1060 mm, a second moment of area of 0.76 m^4 , and a total cross-sectional area of 5.2 m^2 . A Young’s Modulus for concrete is assumed as 34 GPa. Hypothetical sensors A and B are placed at the left and right hand support locations, respectively to record rotations under a 40 tonne 5 axle moving vehicle loading. The damage is simulated as a 30% reduction in stiffness over a 1 m length (5% of the bridge span) at the quarter span location (Figure 11).

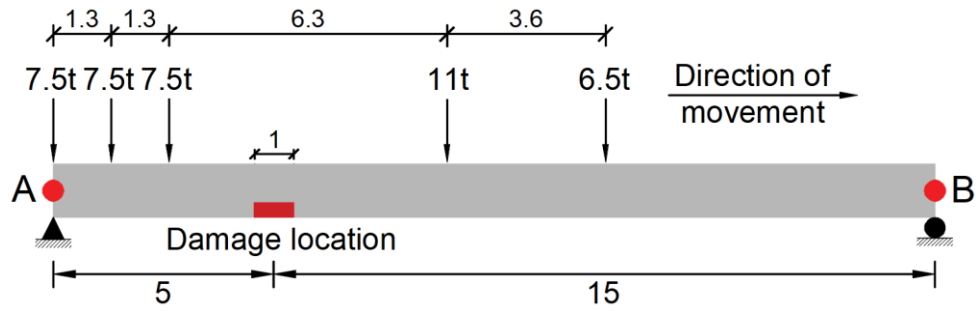


Figure 11. Sketch of 20 m long 1-D simply supported bridge model subject to 5-axle vehicle loading, with rotation sensors at A and B.

Figure 12 (a) gives the rotation responses for the healthy and damaged bridge cases as the 5-axle vehicle loading is moved incrementally across the bridge. The differences between the rotation time histories (Δ Rotation) are given in Figure 12 (b). In this case, it is difficult to identify the damage location accurately from Figure 12 (b) since the plot is no longer triangular and the largest amplitude occurs away from the damage location. This is because each plot in Figure 12(b) is in effect the sum of 5 separate triangles, as illustrated in Figure 12(c).

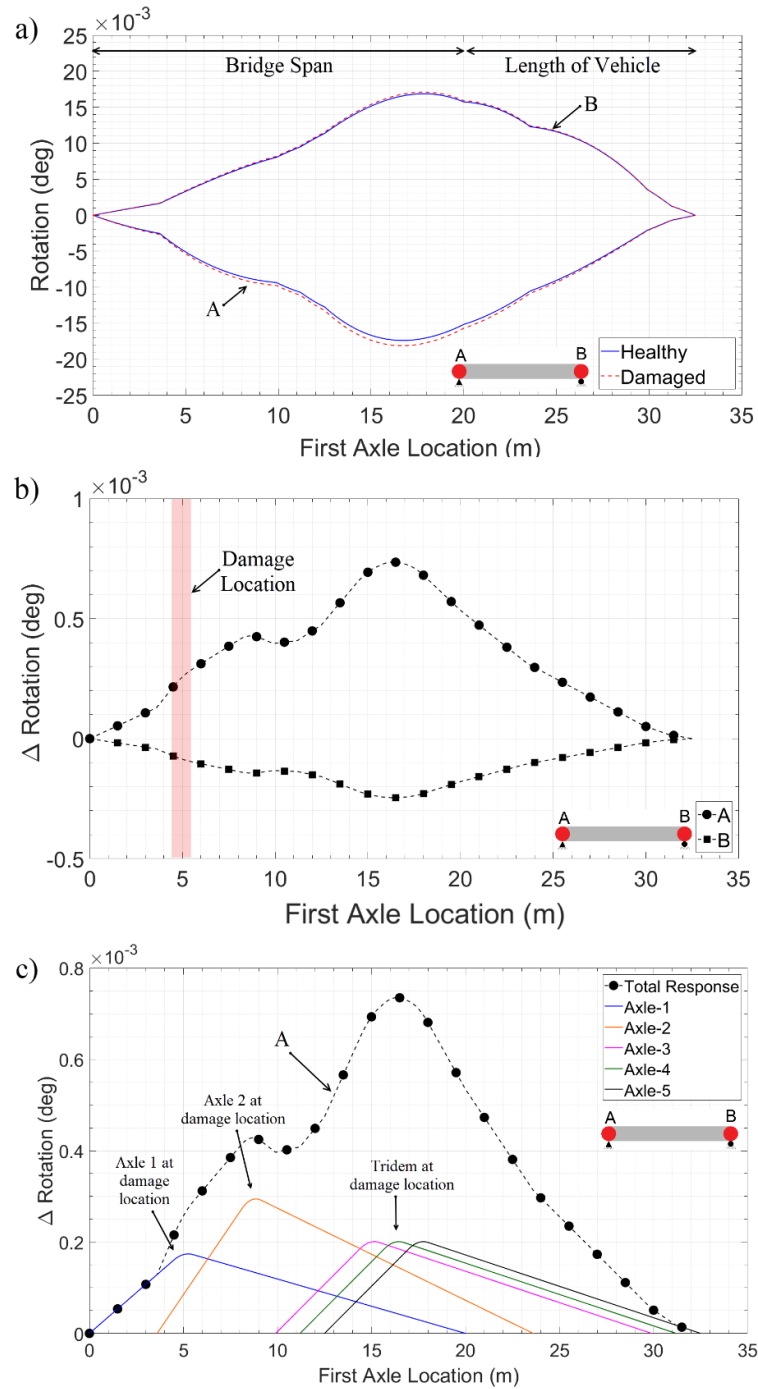


Figure 12. Simulation of rotation responses to 5-axle vehicle loading (a) Response for healthy and damaged bridge cases for sensor locations A and B, (b) Difference in rotation measurements between healthy and damaged states (c) Difference in rotation measurements at A and contributions to the difference from each axle.

It is proposed in this study to back-calculate the rotation influence line (IL) of the bridge from its response to the vehicle. As the IL is the response to a unit load, the difference between healthy and damaged ILs will be triangular. Obtaining the IL is possible (McNulty & OBrien, 2003; Moses, 1979; OBrien, Quilligan, & Karoumi, 2006; Yamaguchi, Kawamura, Matuso, Matsuki, & Naito, 2009), if the axle weights and spacings are known, as would be the case if a Weigh-In-Motion system were present. Here, the rotation ILs are calculated using a process described by OBrien et al (2006). Figure 13(a) depicts the ILs for the two sensor locations (i.e. two supports). The continuous blue curves are for the healthy bridge case and the dashed red curves are for the damaged bridge case. The increase in the amplitude of the unit rotation response is due to the presence of damage. Figure 13(b) shows the difference between calculated ILs (Healthy – Damaged). As expected, the difference is triangular with the maximum amplitude at $L/4$ span, where the damage is simulated.

In practice, rotation influence lines (IL) can be obtained using the procedure described by OBrien et al (2006). This procedure takes the deformation response of a bridge, in any form, and back-calculates the response of the bridge to a unit axle load. To do so, certain information is required as an input into the algorithm such as axle weights, axle configuration and the speed of the traversing vehicle which could be obtained either during a load test or if Bridge Weigh-In-Motion axle detecting sensors are present at the bridge site.

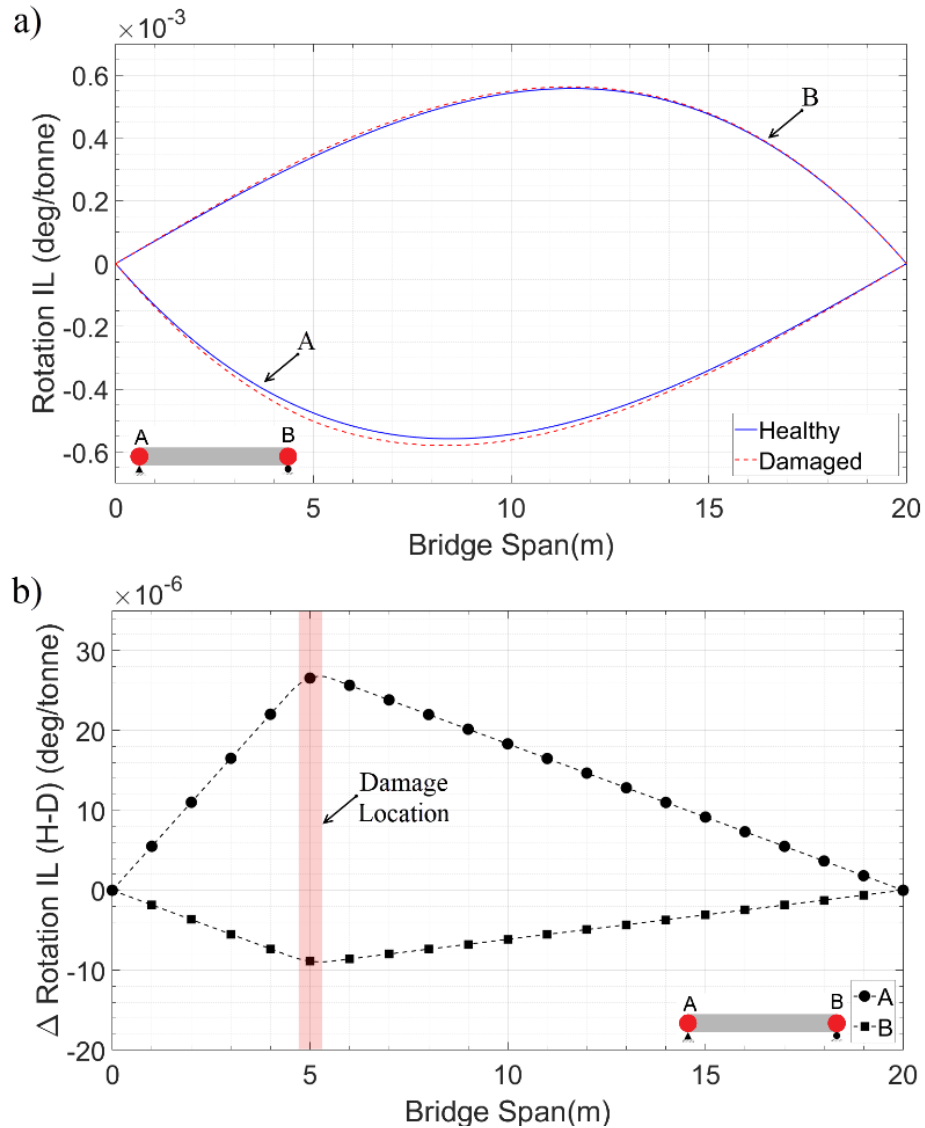


Figure 13. Effect of damage on calculated rotation influence lines (a) Rotation influence line (b) Difference in rotation influence lines for healthy and damaged states.

Figure 14 presents a flowchart highlighting the steps in the proposed damage detection methodology. The idea is to first conduct a careful inspection of the bridge using traditional methods and to use responses to passing traffic to collect the ‘reference’ or ‘healthy’ rotation influence line (Process Nos. 1 and 2). The system of

continuous SHM of the bridge will consist of rotation monitoring (Process No. 3) and elements of Bridge Weigh-In-Motion (WIM) technology to extract the axle spacings and relative axle weights of passing vehicles (Process No. 4). The rotation monitoring system provides the response of the bridge to each passing vehicle which, together with the relative axle weights and spacings are used to calculate the rotation IL of the structure in real time (i.e. current state) (Process No. 5). Any possible damage to the bridge is identified by evaluating the difference between the rotation IL for the reference and current states (Process No. 6).

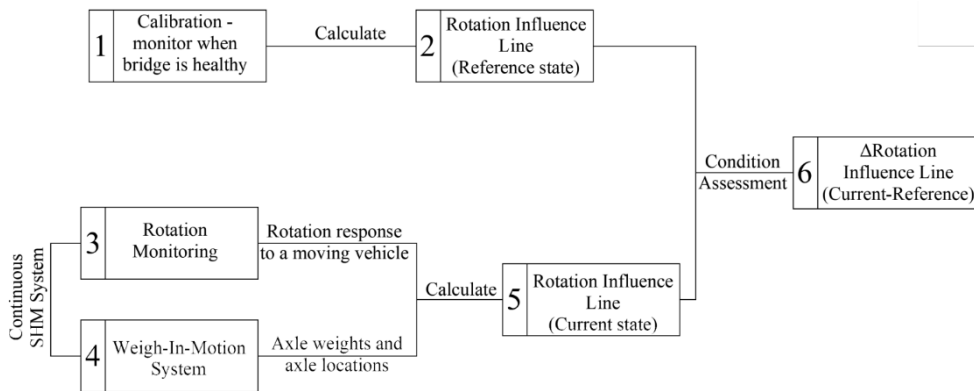


Figure 14. Flowchart highlighting the steps of the proposed methodology.

The methodology proposed in this study focuses on the effect of local damage in a bridge such as would occur due to a bridge strike. The stiffness of a bridge can also vary due to ambient conditions (i.e. temperature and humidity). Unlike local damage, the effect of temperature and humidity is global, i.e., is distributed along the length of the bridge. Temperature change for example, is likely to be similar through the length of the deck and therefore to have a similar effect on (concrete) stiffness through the length. In such a case, the difference in rotation responses would be reasonably uniform and certainly would not be triangular in shape.

In this section, the effect of damage on the bridge structure is studied using a 1-D model, but detecting damage is clearly more challenging for a full 3-D bridge, as will be demonstrated in the next sections.

3.2 Three-Dimensional Finite Element Model

3.2.1 Bridge model

The next bridge modelled is of beam-and-slab construction with precast concrete beams and a continuous structural slab connecting them (Figure 15). Young's modulus for the beams is set at $34 \times 10^9 \text{ N/m}^2$ assuming to be high strength precast, while $31 \times 10^9 \text{ N/m}^2$ is assumed for the in-situ slab. In both cases, a Poisson ratio of 0.15 and material density of 2500 kg/m^3 is assumed. The structure is 20 m long and 10 m wide; representing a short-span bridge with two lanes and narrow shoulders. Sensor locations A-F and the path to be travelled by the vehicle across the bridge are also indicated in the figure.

The model comprises 10 longitudinal beams spaced at 1 m centres and located symmetrically with respect to the bridge centreline. Beams have a constant depth of 0.9 m, resulting in a second moment of area (I) of 0.0685 m^4 . The 0.16 m thick slab is modelled using 1 m x 1 m plate elements, with the exception of those closest to the edge that are 1 m x 0.5 m. An overall structural damping of 3% is considered. The fundamental natural frequency of the bridge is 6.13 Hz and has the mode shape of a half sine in the longitudinal direction.

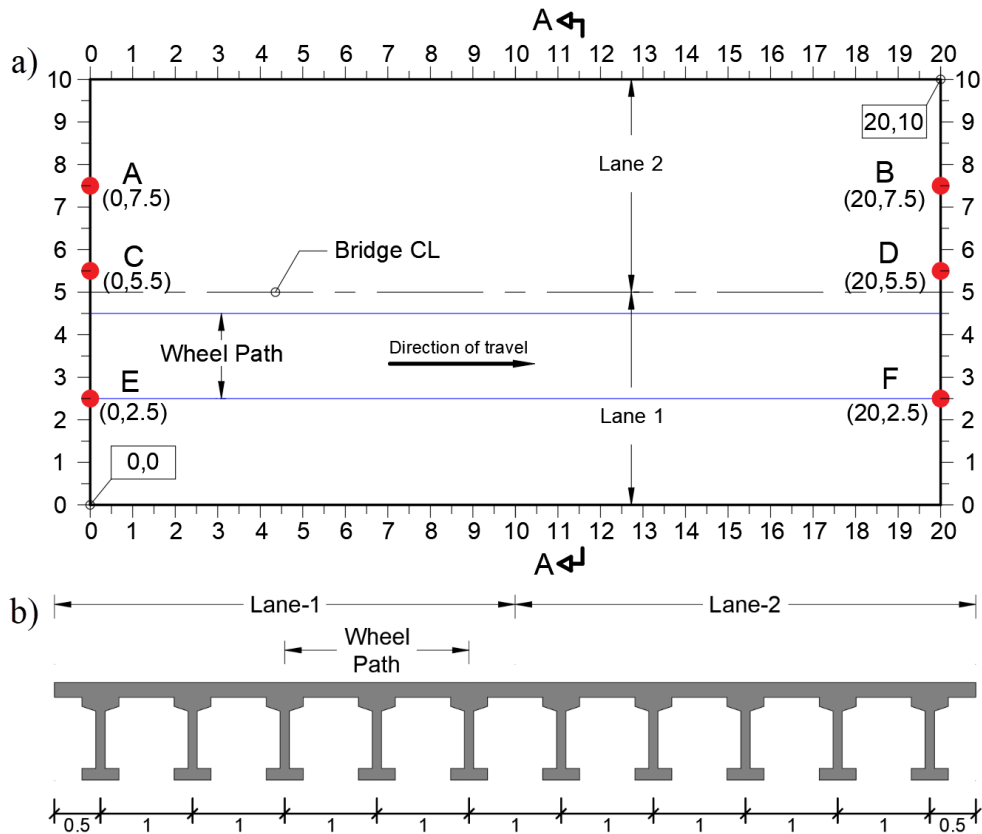


Figure 15. Schematic of bridge modelled in simulations (coordinates and dimensions in m) (a) Plan view (b) Cross – section (Section A-A)

3.2.2 Vehicle model

The vehicle is a typical European 5-axle truck with a rear tridem. It consists of two rigid bodies, with masses and springs and a hinge, as shown in Figure 16. The overall length of the truck, including front and rear frame overhangs, is 14.9 m. The axle spacings are 3.6, 6.33, 1.31 and 1.31 m respectively from front to back wheel. The transverse distance between the two wheels of each axle is 2 m. Two truck configurations are tested, with the same geometry but different total weight. For the first truck model, denoted V40 (full-loaded truck), the gross vehicle weight (GVW) is 40

tonnes while, for the second truck model, denoted V25 (half-loaded truck), the GVW is 25 tonnes. Individual axle weights are provided in Table 1.

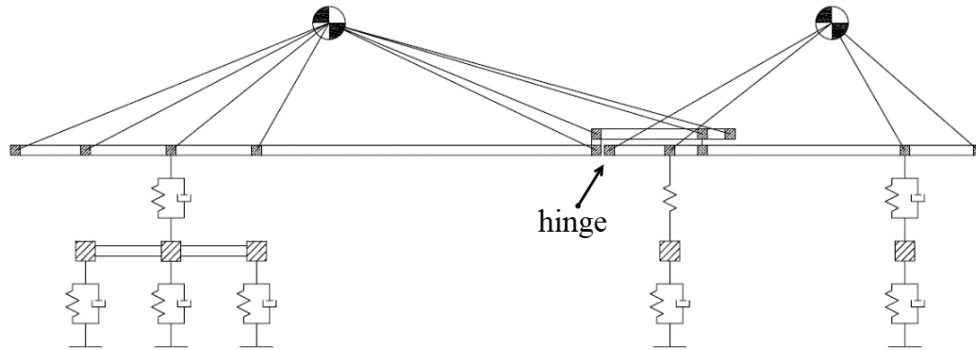


Figure 16. Five axle vehicle model.

Table 1. Vehicle axle weights in tonnes

Axle No.	1 st	2 nd	3 rd	4 th	5 th	GVW
V40	6.5	11	7.5	7.5	7.5	40
V25	5.9	7.1	4	4	4	25

All axles are assumed to have steel suspensions except the 2nd, which is assumed to have air suspensions. Viscous damping is considered to be zero for the air suspension. Single tires are assumed in the 1st axle and doubles elsewhere. The main properties of the truck are shown in Table 2 (Henning, Nielsen, & Enevoldsen, 1997). Given these properties, body frequencies of vehicle V40 range from 1.4 to 2.9 Hz and axle roll and hop frequencies range between 10.5 and 15.6 Hz. In the case of vehicle V25, due to the change in the GVW, body frequencies can be found in a different range, namely from 1.9 to 4.1 Hz.

Table 2. Suspension and tyre parameters

Parameter	Value
Steel suspension stiffness (N/m)	1.8×10^6
Air suspension stiffness (N/m)	5×10^5
Suspension viscous damping (N·s/m)	5×10^3
Tyre stiffness, 1 st axle (N/m)	1×10^6
Tyre stiffness, 2 nd to 5 th axles (N/m)	2×10^6
Tyre damping (N·s/m)	3×10^3

3.2.3 Numerical simulations

The 5th and 6th authors carried out 12 numerical simulations and returned the results as ‘blind’ i.e. the 1st-4th authors did not know the location or severity of the damage a priori. However, responses for four calibration runs were provided, for which the bridge was known to be healthy. The goal was to test if the algorithm was able to identify/quantify damage for the twelve blind signals.

In all simulations, vehicle-bridge interaction is implemented using a Lagrange multiplier technique (Gonzalez, 2010). This is applied to ensure compatibility of equations for the vehicle and the bridge at the contact points. The Lagrange multiplier is incorporated by modifying the bulk file of the system containing the model information about vehicle and bridge prior to solving the transient problem. In order to dynamically excite the truck before entering the bridge, a 50 m approach road with a small bump at the beginning is simulated. In the simulations, the road profile is assumed to be a ‘very good’ (Class A) profile typical of pavements found on well-maintained highways. The profile consists of 101 spatial waves between 0.01 cycles/m and 4 cycles/m with a geometric spatial mean of 0.5×10^{-6} m³/cycle and phases randomly generated for each wave. The vehicle moves from left to right, with the left wheels travelling over the beam placed at 4.5 m and the right wheels, over the beam placed at

2.5 m (see Figure 15). The rotation response of the structure is recorded at six locations, three at the left-hand end of the deck (A, C and E) and three at the right-hand end of the deck (B, D and F). Details of the calibration runs are provided in Table 3. In this study, the calibration data is used to obtain the reference bridge state and is collected when the bridge has been confirmed by conventional means as being healthy.

Table 3. Calibration run data

Calibration Test No.	Speed (m/s)	Vehicle Type
1	20	V40
2	20	V25
3	30	V40
4	30	V25

Table 4 shows the parameters for the other 12 simulations. However, prior to testing the damage detection algorithm only the data in the first three columns (unshaded) in the table were provided to the analyst. Blind test No 1 (Table 4) can be visualised in Figure 17(a), where the fully loaded truck (V40) is travelling at 20 m/s in Lane 1 when there is road profile type 1 on the bridge. The damage is simulated at 3L/8 span location as 12.1% reduction in stiffness over 3 m length and 5 m width (i.e. damage entirely situated at lane – 1). For demonstrations purposes, Figure 17 (b) and (c) illustrate the blind test simulation Nos. 2 and 3 respectively. To check for potential false positives, in blind test simulation No 4 the bridge was simulated as being healthy but the analyst was not told this a priori.

Damage is modelled as a percentage stiffness loss at the selected beam elements, while the slab is assumed to remain intact in all cases. The longitudinal location given in Table 4 corresponds to the centre of the damage in the affected beams, which extends

longitudinally 1.5 m both sides of the centre. The damage values are calculated with respect to the bending stiffness (modulus of elasticity multiplied by second moment of area) of the entire cross-section. The profile labelled as ‘1’ is the same as that used in the calibration runs whereas profiles labelled ‘2’ and ‘3’ are randomly generated with geometric spatial means of 2×10^{-6} and 8×10^{-6} m³/cycle, respectively. This was to investigate if the effectiveness of the approach is sensitive to a change in road profile on the bridge after the healthy influence line has been calculated.

Table 4. Blind test data parameters

Provided Data			Blind Data				
Test no.	Vehicle		Road Profile	Damage			Stiffness loss (%)
	Speed (m/s)	Type		Longitudinal	Transverse		
				Location (m)	Lane position	Width (m)	
1	20	V40	1	3L/8	1	5	12.1%
2	30	V40	1	L/2	2	5	10.0%
3	20	V40	1	L/3, 3L/4	1&2, 1	10, 5	11.9%, 12.1 %
4	30	V25	3	Healthy			
5	20	V40	1	5L/8	1	5	8.0%
6	30	V25	1	L/8	1	5	12.1%
7	20	V25	1	5L/8	1&2	10	16.0%
8	20	V25	1	L/2	2	5	6.0%
9	30	V40	1	5L/8	2	5	8.0%
10	30	V25	1	2L/3	1&2	10	16.0%
11	20	V40	2	3L/4	2	5	8.0%
12	30	V25	1	3L/8, 2L/3	1&2, 1	10, 5	24.2%, 8.0%

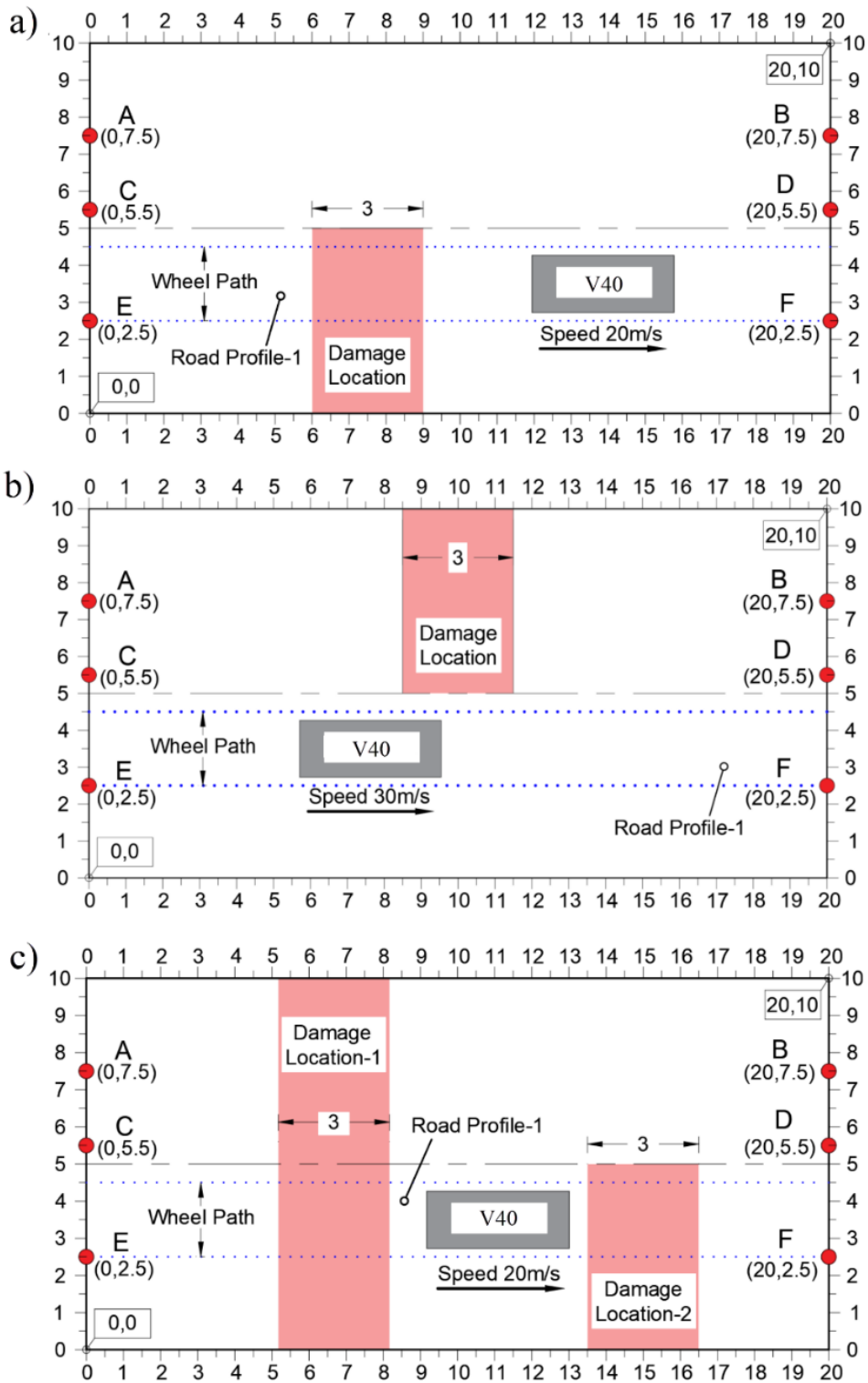


Figure 17. Schematic views of blind test simulations (a) Test 1 (b) Test 2 (c) Test 3.

3.3 Calculating influence lines from the raw rotation signal

The rotation influence lines for the healthy bridge model are calculated for each sensor location (A-F in Figure 15(a)) using the responses provided to the calibration runs. Figure 18(a) shows the rotation time history obtained from sensor F for calibration run 1 (Table 3), this signal is typical of the signals obtained for other calibration runs and for other sensor locations. The continuous blue curve is the raw rotation signal due to the 5-axle vehicle travelling in the path indicated in Figure 15. It is clear from the raw signal that the response consists of both static and dynamic components. Initially, a moving average filter is applied to the raw signal to remove high frequency oscillation due to bridge vehicle dynamic interaction. The filtered rotation data is plotted in red in Figure 18(a). This filtered data is used to calculate the rotation influence line of the bridge. The resulting influence line for sensor location F (for the vehicle path indicated in Figure 15) is the uppermost plot in Figure 18(b). The influence lines for the other sensor locations, found in a similar way, are also plotted. The contributions of each axle to the total bridge response can be calculated using these influence lines and the known axle weights, and for completeness these are shown as dashed plots in Figure 18(a).

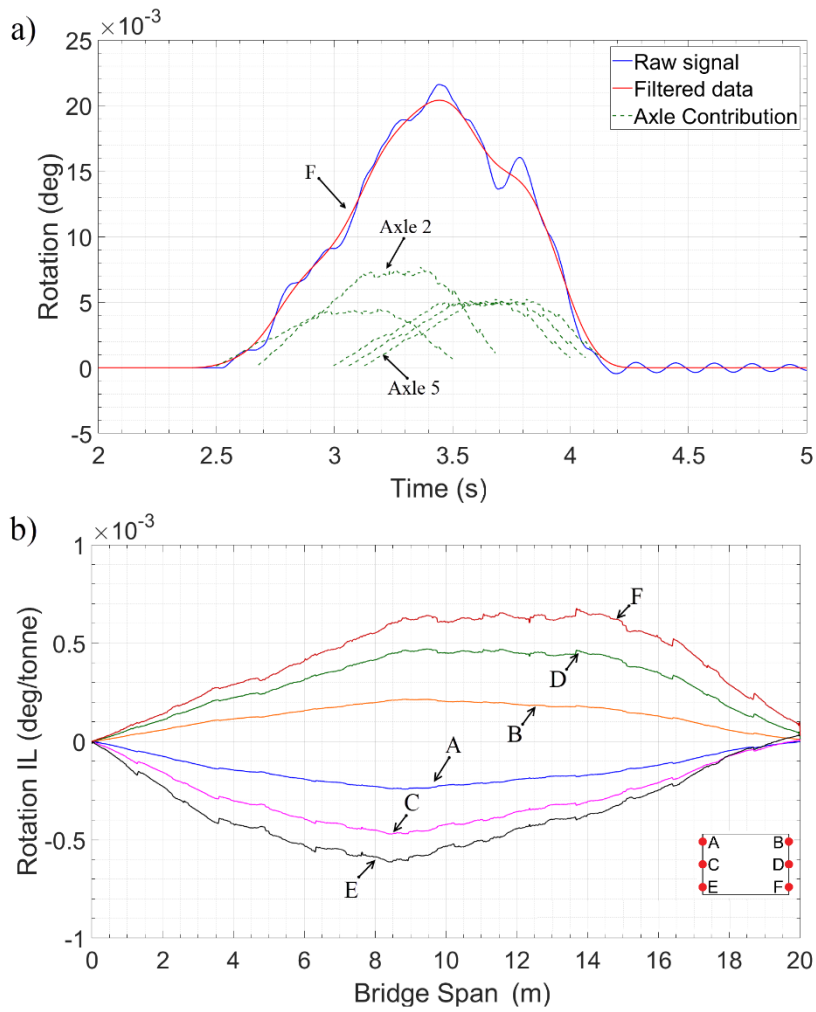


Figure 18. Results from calibration run No 1, (a) Rotation time history for Sensor F due to a 5-axle truck and contribution of each axle (b) Calculated rotation influence lines for each sensor.

3.4 Results of blind tests and further discussion

Rotation influence lines obtained at each sensor location for the blind test simulations are used to assess the condition of the 3-D bridge model. In these analyses, calibration data are used to determine the reference bridge (healthy) condition. Figure 19(a) presents the results obtained from the calibration (continuous) and blind test

simulation No. 1 (dashed). A small but clear increase in rotation ILs can be seen, suggesting damage in the bridge. The increase in the amplitude of rotation influence line is most significant at Sensor location E suggesting damage near that sensor. This was subsequently confirmed – damage was in Lane 1 at $3L/8$, and it was also in the same lane as the travelling vehicle.

Figure 19 (b) shows the rotation IL difference between the calibration runs and blind test simulation No.1. The rotation IL difference plots are triangular with a maximum amplitude of around 32×10^{-6} deg/tonne at approximately 8.5 m from the left-hand support. The damaged zone predicted by the algorithm is indicated in Figure 19(b). Sensors E and F show the largest amplitude which indicates that the damage is likely to be on the side of Lane 1 where they are located. Damage in this test is, indeed, in Lane 1 at $3L/8$. The match between actual and predicted (longitudinal) location of damage is good, as can be seen in the figure.

Figure 20 presents the results from blind test simulation Nos. 2 – 4. In simulation No. 2, the damage is at midspan on the Lane 2 side of the bridge and is a 10% reduction in stiffness over 3 m. It is clearly visible in Figure 20 (a) that the maximum amplitude of difference in rotation influence line occurs at midspan. The predicted damage extent is a little greater, being 1 m longer than the actual length of damage. The maximum amplitude of difference in rotation influence lines are obtained from sensors A, C, D, B which are located on the bridge centre line at the Lane 2 side of the bridge. This indicates, correctly, that the location of damage is likely in Lane 2.

The maximum difference in rotation influence lines obtained from test No. 2 is approximately 5×10^{-6} deg/tonne. Although the severity of damage simulated in this test is close enough to that of Test No. 1, the magnitudes of the changes in rotation influence lines vary significantly. This is because, in Test No. 1 damage is in the lane where the

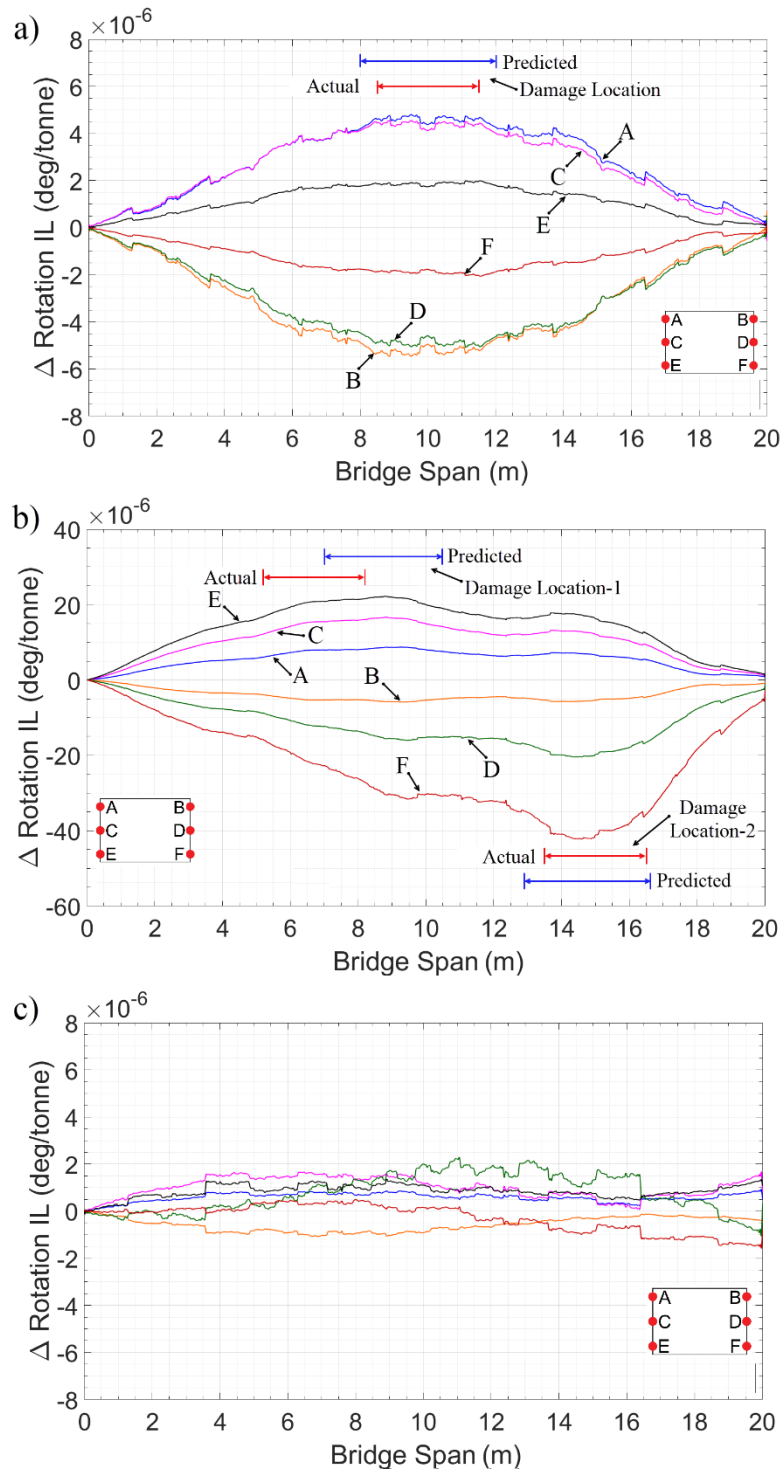


Figure 20. Difference in rotation influence line plots for blind test data. (a) Test 2 (b) Test 3 (c) Test 4.

Figure 20 (b) shows the results obtained from Test No. 3. This time, for all sensors, there are two peaks in the influence line difference plots, indicating damage at two separate locations. The first peak is observed around 8.75 m and the second at approximately 14.75 m from the left-hand support. The second damage location is identified accurately but for the first damage there is a 2 m offset between the predicted and actual damage locations. The locations of damage across the width of the bridge are predicted by examining the relative magnitudes for each sensor location. Since the maximum amplitudes for both peak locations are obtained from sensors E and F, damage is deemed to be in the Lane 1 side of the bridge. Admittedly damage at the first peak location is actually across the full width of the bridge, but it was hard to discern this by looking at the figure.

The results obtained from the Test No. 4 are presented in Figure 20(c). It is clearly visible in the figure that the shape of the plot is almost constant which implies a healthy bridge condition. The magnitudes of rotation IL differences obtained from each sensor are in a range of $\pm 2 \times 10^{-6}$ deg/tonne which is significantly less than the corresponding results observed in the previous simulations. The only difference in defined parameters between Test No. 4 and the calibration runs, is a change in road profile (see Table 4) and the resulting difference in the plots was deemed to be due to the change in road profile.

Figure 21 summarises the results obtained from all 12 blind test simulations. The blue and red lines in the figure represent the predicted and actual damage extents along the length of the bridge model, respectively. It is shown in the figure that the proposed damage detection method successfully identifies the presence of damage in all blind test simulations, even if the prediction of extent/location is not always accurate, particularly for the more complicated damage scenarios. In summary, all blind test simulations

where damage was simulated are identified as damaged, and the one healthy simulation in the blind test data (Test No. 4) was correctly identified as undamaged. In only one case (No. 12) there was a failure to identify one of two damages. As a general trend, the predicted damage extent is slightly more conservative than the actual extent of damage. In some of the tests, where damage is modelled across the full width of the bridge (i.e. Test Nos. 3, 7, 10 and 12), it was not possible to identify damage on the Lane-2 side. This is because, for all blind test data provided to authors seeking to detect damage, the vehicle was positioned only in Lane 1. Hence, the effect of damage on the Lane 2 side of the bridge was more difficult to detect. In Test No. 12, where damage is simulated at two locations (i.e. at $3L/8$ and $2L/3$ span locations), it was not possible to detect damage simulated at the $2L/3$ span location. The severity of damage modelled at the $3L/8$ location is 24.2% across the full width of the bridge, whereas at $2L/3$ the severity of damage is much less (i.e. 8%) and occurs only on the Lane 1 side of the structure. Since the damage locations are close to each other with significantly varying severities, the effect of damage at the $2L/3$ span location, was not evident in the rotation IL difference plot (i.e. it was hidden by the effect of damage at $3L/8$ span location). This is illustrated in Figure 22. Overall, Figure 21 confirms that the proposed damage detection method identifies the condition of the bridge reasonably well and is a promising tool for evaluating the condition of bridge structures.

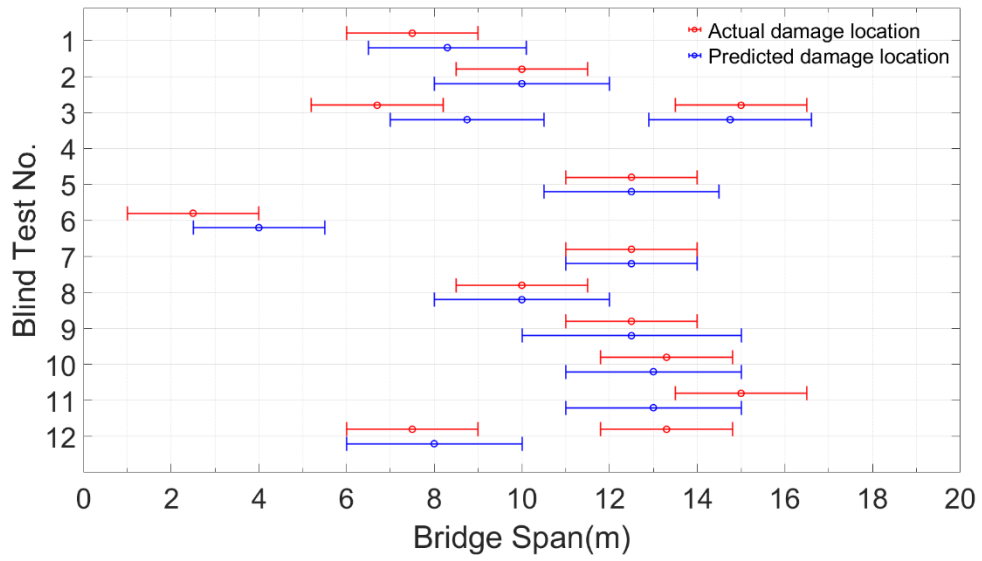


Figure 21. Summary of results: simulated and predicted damage locations for 12 blind test simulations.

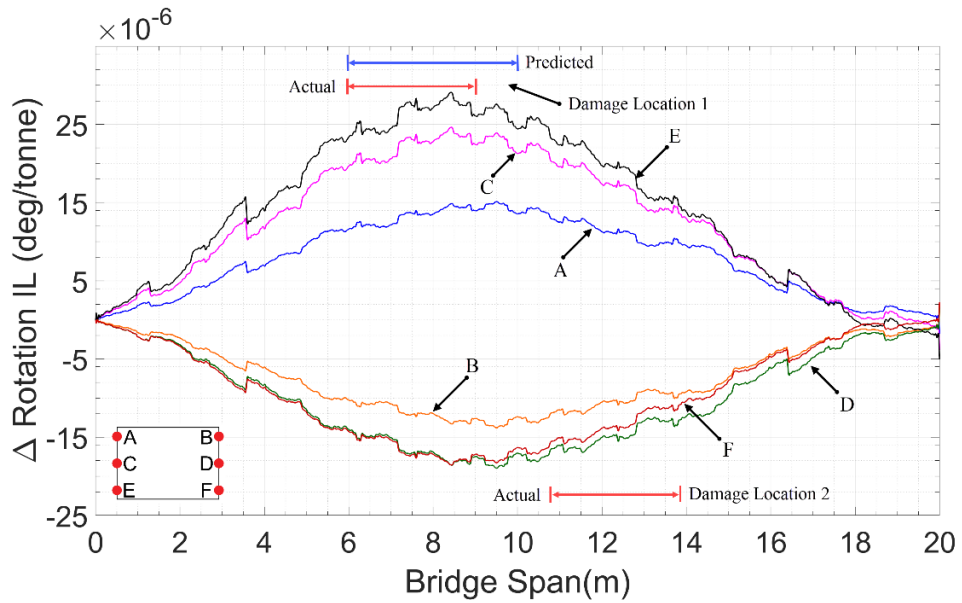


Figure 22. Difference in predicted rotation influence lines for calibration and blind test No-12.

4 Conclusion

This paper develops a novel bridge condition assessment methodology using rotation measurements. Initially numerical and experimental analysis are carried out to investigate the sensitivity of rotation as a parameter to identify damage on bridge type structures. Numerical analyses carried out on a 1-D bridge model provide the theoretical basis of the proposed damage detection method and the difference in rotation influence lines between healthy and damaged bridges is proposed as a damage indicator. Following this, a 3-D bridge dynamic FE vehicle bridge dynamic interaction model is developed, and the proposed damage detection method is tested under more realistic conditions using 12 blind test simulations. The method accurately evaluated the bridge condition for all 12 blind test simulations. The following conclusions can be drawn from this study:

- Rotation is a sensitive parameter for identifying damage in a bridge structure. In essence, if damage occurs, either locally or globally, it results in an increase in the magnitude of rotation measurements.
- Difference in rotation influence lines obtained for healthy and damaged states using the response of a bridge to a vehicle of known weight, can successfully identify damage and its location.
- For simply supported bridge structures the most effective sensor locations to identify damage are supports, where the maximum amplitude of rotations occurs.
- A sensor placed at a support location closer to a damage location is more sensitive to damage than a sensor placed at a remote location.

- The method is more effective when the vehicle passes close (transversely) to the damage location.

5 Acknowledgements

This research project has received funding from the European Union's Horizon 2020 research and innovation programme under the Marie Skłodowska– Curie grant agreement No. 642453.

References

- Alten, K., Ralbovsky, M., Vorwagner, A., Toplitzer, H., & Wittmann, S. (2017). Evaluation of Different Monitoring Techniques During Damage Infliction on Structures. *Procedia Engineering*, *199*, 1840–1845. <https://doi.org/10.1016/j.proeng.2017.09.106>
- American Association of State Highway and Transportation Officials. (2012). *AASHTO LRFD Bridge Design Specifications* (6th ed.).
- Andersen, J. E., Enckell, M., Alcover, I. F., & Chryssanthopoulos, M. K. (2013). The Structural Health Monitoring System of the Izmit Bay Bridge : overview and SHM-based fatigue assessment. In *Second Conference on Smart Monitoring, Assessment and Rehabilitation of Civil Structures*. Istanbul.
- Antunes, P. F. C., Marques, C. A., Varum, H., & Andre, P. S. (2012). Biaxial Optical Accelerometer and High-Angle Inclinometer With Temperature and Cross-Axis Insensitivity. *IEEE Sensors Journal*, *12*(7), 2399–2406. <https://doi.org/10.1109/JSEN.2012.2190763>

- Bas, S., Apaydin, N. M., Ilki, A., & Catbas, F. N. (2018). Structural health monitoring system of the long-span bridges in Turkey. *Structure and Infrastructure Engineering*, 14(4), 425–444. <https://doi.org/10.1080/15732479.2017.1360365>
- Bradley, M., González, A., & Hester, D. (2010). Analysis of the structural response to a moving load using empirical mode decomposition (pp. 117–117). London: Taylor & Francis. <https://doi.org/10.1201/b10430-49>
- Bruns, D. G. (2017). An optically referenced inclinometer with sub-microradian repeatability. *Review of Scientific Instruments*, 88(11), 115111. <https://doi.org/10.1063/1.5010202>
- Burdet, O., & Zanella, J.-L. (2000). Automatic Monitoring of Bridges using Electronic Inclinometers. *IABSE Congress Report*, 16(6), 1574–1581. <https://doi.org/10.2749/222137900796314284>
- Cardini, A. J., & DeWolf, J. T. (2009). Long-term Structural Health Monitoring of a Multi-girder Steel Composite Bridge Using Strain Data. *Structural Health Monitoring: An International Journal*, 8(1), 47–58. <https://doi.org/10.1177/1475921708094789>
- Chang, C.-I., Tsai, M.-H., Liu, Y.-C., Sun, C.-M., & Fang, W. (2011). Design and implementation of an extremely large proof-mass CMOS-MEMS capacitive tilt sensor for sensitivity and resolution improvement. In *2011 16th International Solid-State Sensors, Actuators and Microsystems Conference* (pp. 1104–1107). IEEE. <https://doi.org/10.1109/TRANSDUCERS.2011.5969190>
- Concast Precast Group Concrete Prestressed Girders Technical Guide. (2009).

Retrieved from
http://www.concastprecast.co.uk/images/uploads/brochures/Concast_Civil.pdf

Crescini, D., Marioli, D., Romani, M., Sardini, E., & Taroni, A. (2004). An inclinometer based on free convective motion of a heated air mass. In *ISA/IEEE Sensors for Industry Conference* (pp. 11–15). IEEE.
<https://doi.org/10.1109/SFICON.2004.1287118>

Erdenebat, D., Waldmann, D., Scherbaum, F., & Teferle, N. (2018). The Deformation Area Difference (DAD) method for condition assessment of reinforced structures. *Engineering Structures*, *155*(September 2017), 315–329.
<https://doi.org/10.1016/j.engstruct.2017.11.034>

Fração, O., Falate, R., Fabris, J. L., Santos, J. L., Ferreira, L. A., & Araújo, F. M. (2006). Optical inclinometer based on a single long-period fiber grating combined with a fused taper. *Optics Letters*, *31*(20), 2960. <https://doi.org/10.1364/OL.31.002960>

Glišić, B., Posenato, D., Inaudi, D., & Figini, A. (2008). Structural health monitoring method for curved concrete bridge box girders. In M. Tomizuka (Ed.), *Proc. SPIE 6932, Sensors and Smart Structures Technologies for Civil, Mechanical, and Aerospace Systems* (Vol. 693204). International Society for Optics and Photonics.
<https://doi.org/10.1117/12.778643>

Gonzalez, A. (2010). Vehicle-Bridge Dynamic Interaction Using Finite Element Modelling. In *Finite Element Analysis*. Sciyo. <https://doi.org/10.5772/10235>

Haritos, N., & Chalko, T. J. (1996). Determination of abutment support conditions in an 80-year-old RC bridge. In S. B. Chase (Ed.), *Proc. SPIE 2946, Nondestructive*

Evaluation of Bridges and Highways (Vol. 2946, pp. 312–323). International Society for Optics and Photonics. <https://doi.org/10.1117/12.259148>

He, X., Yang, X., & Zhao, L. (2014). Application of Inclinometer in Arch Bridge Dynamic Deflection Measurement. *Indonesian Journal of Electrical Engineering and Computer Science*, 12(5), 3331–3337.

Heitner, B., O'Brien, E.J., Yalams, T., Schoefs, F., Leahy, C., Décatore, R. (2019), 'Updating probabilities of bridge reinforcement corrosion using health monitoring data', *Engineering Structures*, 190(2019), 1st July, 41-51, doi: 10.1016/j.engstruct.2019.03/103

Helmi, K., Taylor, T., Zarafshan, A., & Ansari, F. (2015). Reference free method for real time monitoring of bridge deflections. *Engineering Structures*, 103, 116–124. Retrieved from <http://www.sciencedirect.com/science/article/pii/S0141029615005659>

Henning, P. K., Nielsen, S. R. K., & Enevoldsen, I. (1997). *Heavy Vehicles on minor highway bridges – Dynamic modelling of vehicles and bridges*. In: *Report in Department of Building technology any and Structural Engineering*.

Hester, D., & González, A. (2012). A wavelet-based damage detection algorithm based on bridge acceleration response to a vehicle. *Mechanical Systems and Signal Processing*, 28, 145–166. <https://doi.org/10.1016/j.ymsp.2011.06.007>

Hou, X., Yang, X., & Huang, Q. (2005). Using Inclinometers to Measure Bridge Deflection. *Journal of Bridge Engineering*, 10(5), 564–569. [https://doi.org/10.1061/\(ASCE\)1084-0702\(2005\)10:5\(564\)](https://doi.org/10.1061/(ASCE)1084-0702(2005)10:5(564))

- Hoult, N. A., Fidler, P. R. A., Hill, P. G., & Middleton, C. R. (2010). Long-Term Wireless Structural Health Monitoring of the Ferriby Road Bridge. *Journal of Bridge Engineering*. Retrieved from wos:000274522600004
- Huang, N. E., Huang, K., & Chiang, W.-L. (2005). HHT based bridge structural health-monitoring method. In *Hilbert-Huang Transform and Its Applications* (Vol. Volume 5, pp. 263–287). WORLD SCIENTIFIC. https://doi.org/10.1142/9789812703347_0012
- Inaudi, D., & Glisic, B. (2002). Interferometric inclinometer for structural monitoring. In *15th Optical Fiber Sensors Conference Technical Digest*. (Vol. 1, pp. 391–394). IEEE. <https://doi.org/10.1109/OFS.2002.1000635>
- Ko, J. M. M., & Ni, Y. Q. (2005). Technology developments in structural health monitoring of large-scale bridges. *Engineering Structures*, 27(12 SPEC. ISS.), 1715–1725. <https://doi.org/10.1016/j.engstruct.2005.02.021>
- Li, H., & Ou, J. (2016). The state of the art in structural health monitoring of cable-stayed bridges. *Journal of Civil Structural Health Monitoring*, 6(1), 43–67. <https://doi.org/10.1007/s13349-015-0115-x>
- Li, Z. H., & Au, F. T. K. (2014). Damage Detection of a Continuous Bridge from Response of a Moving Vehicle. *Shock and Vibration*, 2014, 1–7. <https://doi.org/10.1155/2014/146802>
- Liu, S., & Zhu, R. (2017). Micromachined Fluid Inertial Sensors. *Sensors*, 17(2), 367. <https://doi.org/10.3390/s17020367>
- LLoret, S., Inaudi, D., & Vurpillot, S. (1998). <title>Static and dynamic bridge

monitoring with fiber optic sensors</title>. In S. Huang, K. D. Bennett, & D. A. Jackson (Eds.), *Proc. SPIE 3555, Optical and Fiber Optic Sensor Systems* (Vol. 3555, pp. 136–146). International Society for Optics and Photonics. <https://doi.org/10.1117/12.318201>

McNulty, P., & O'Brien, E. (2003). Testing of Bridge Weigh-In-Motion System in a Sub-Arctic Climate. *Journal of Testing and Evaluation*, 31(6), 11686. <https://doi.org/10.1520/JTE12377J>

Moses, F. (1979). Weigh-in-Motion System Using Instrumented Bridges. *Transportation Engineering Journal of ASCE*, 105(3), 233–249. Retrieved from <http://cedb.asce.org/CEDBsearch/record.jsp?dockey=0008759>

O'Leary, P., & Harker, M. (2012). A Framework for the Evaluation of Inclinometer Data in the Measurement of Structures. *IEEE Transactions on Instrumentation and Measurement*, 61(5), 1237–1251. <https://doi.org/10.1109/TIM.2011.2180969>

O'Brien, E., Carey, C., & Keenahan, J. (2015). Bridge damage detection using ambient traffic and moving force identification. *Structural Control and Health Monitoring*, 22(12), 1396–1407. <https://doi.org/10.1002/stc.1749>

O'Brien, E. J., Quilligan, M. J., & Karoumi, R. (2006). Calculating an influence line from direct measurements. *Proceedings of the Institution of Civil Engineers - Bridge Engineering*, 159(1), 31–34. <https://doi.org/10.1680/bren.2006.159.1.31>

Olaru, R., & Cotae, C. (1997). Tilt sensor with magnetic liquid. *Sensors and Actuators A: Physical*, 59(1–3), 133–135. [https://doi.org/10.1016/S0924-4247\(97\)80162-8](https://doi.org/10.1016/S0924-4247(97)80162-8)

Olaru, R., & Dragoi, D. D. (2005). Inductive tilt sensor with magnets and magnetic

fluid. *Sensors and Actuators A: Physical*, 120(2), 424–428.
<https://doi.org/10.1016/j.sna.2005.01.015>

Park, J., Moon, D.-S., Spencer, B. F., & Sim, S. (2017). Neutral-axis Identification using strain and acceleration measurements. In *The 2017 World Congress on Advances in Structural Engineering and Mechanics (ASEM17)*. Seoul, Korea.

Perregaux, N., Vurpillot, S., Inaudi, D., & Burdet, O. (1998). Vertical Displacement of Bridges using the SOFO System a Fiber Optic Monitoring Method for Structures. In *12th Eng. Mech. Conference "A Force for the 21st Century"*, 17-20.05.1998 (Vol. 05, pp. 17–20). Retrieved from <https://infoscience.epfl.ch/record/111635/files/Perregaux98.pdf>

Robert-Nicoud, Y., Raphael, B., Burdet, O., & Smith, I. F. C. (2005). Model Identification of Bridges Using Measurement Data. *Computer-Aided Civil and Infrastructure Engineering*, 20(2), 118–131. <https://doi.org/10.1111/j.1467-8667.2005.00381.x>

Shoukry, S. N., Riad, M. Y., & William, G. W. (2009). Longterm sensor-based monitoring of an LRFD designed steel girder bridge. *Engineering Structures*, 31(12), 2954–2965. <https://doi.org/10.1016/j.engstruct.2009.07.023>

Sigurdardottir, D. H., & Glisic, B. (2013). Neutral axis as damage sensitive feature. *Smart Materials and Structures*, 22(7), 075030. <https://doi.org/10.1088/0964-1726/22/7/075030>

Sigurdardottir, D. H., & Glisic, B. (2014). Detecting minute damage in beam-like structures using the neutral axis location. *Smart Materials and Structures*, 23(12),

125042. <https://doi.org/10.1088/0964-1726/23/12/125042>

Sigurdardottir, D. H., & Glisic, B. (2015). The neutral axis location for structural health monitoring: an overview. *Journal of Civil Structural Health Monitoring*, 5(5), 703–713. <https://doi.org/10.1007/s13349-015-0136-5>

Sousa, H., Cavadas, F., Henriques, A., Bento, J., & Figueiras, J. (2013). Bridge deflection evaluation using strain and rotation measurements. *Smart Structures and Systems*, 11(4), 365–386. <https://doi.org/10.12989/sss.2013.11.4.365>

Stajano, F., Hout, N., Wassell, I., Bennett, P., Middleton, C., & Soga, K. (2010). Smart bridges, smart tunnels: Transforming wireless sensor networks from research prototypes into robust engineering infrastructure. *Ad Hoc Networks*, 8(8), 872–888. <https://doi.org/10.1016/j.adhoc.2010.04.002>

Steel Construction Institute. (2015). *Steel Building Design: Design Data*. The Steel Construction Institute and The British Constructional Steelwork Association Ltd.

Vurpillot, S., Krueger, G., Benouaich, D., Clément, D., & Inaudi, D. (1998). Vertical Deflection of a Pre-Stressed Concrete Bridge Obtained Using Deformation Sensors and Inclinometer Measurements. *ACI Structural Journal*, 95(5). <https://doi.org/10.14359/566>

Wu, C.-M., & Chuang, Y.-T. (2004). Roll angular displacement measurement system with microradian accuracy. *Sensors and Actuators A: Physical*, 116(1), 145–149. <https://doi.org/10.1016/j.sna.2004.04.005>

Wyler AG. (2016). Levelmatic 31 - High precision analog inclination sensor technical specification. Retrieved from www.wylerag.com

- Yamaguchi, E., Kawamura, S., Matuso, K., Matsuki, Y., & Naito, Y. (2009). Bridge-Weigh-In-Motion by Two-Span Continuous Bridge with Skew and Heavy-Truck Flow in Fukuoka Area, Japan. *Advances in Structural Engineering*, 12(1), 115–125. <https://doi.org/10.1260/136943309787522614>
- Zeinali, Y., & Story, B. (2017). Framework for Flexural Rigidity Estimation in Euler-Bernoulli Beams Using Deformation Influence Lines. *Infrastructures*, 2(4), 23. <https://doi.org/10.3390/infrastructures2040023>
- Zeinali, Y., & Story, B. A. (2018). Impairment localization and quantification using noisy static deformation influence lines and Iterative Multi-parameter Tikhonov Regularization. *Mechanical Systems and Signal Processing*, 109, 399–419. <https://doi.org/10.1016/j.ymsp.2018.02.036>
- Zhang, F. (2004). The accelerometer and tilt sensor based on natural convection gas pendulum. In *International Conference on Information Acquisition* (pp. 122–125). IEEE. <https://doi.org/10.1109/ICIA.2004.1373333>
- Zhang, W. W., Wang, Z. H., & Ma, H. W. (2009). Studies on Wavelet Packet-Based Crack Detection for a Beam under the Moving Load. *Key Engineering Materials*, 413–414, 285–290. <https://doi.org/10.4028/www.scientific.net/KEM.413-414.285>
- Zhang, W., Zhu, H., & Lee, J. E.-Y. (2015). Piezoresistive Transduction in a Double-Ended Tuning Fork SOI MEMS Resonator for Enhanced Linear Electrical Performance. *IEEE Transactions on Electron Devices*, 62(5), 1596–1602. <https://doi.org/10.1109/TED.2015.2414272>

Zhao, L., & Yeatman, E. M. (2007). Micro Capacitive Tilt Sensor for Human Body Movement Detection. In *4th International Workshop on Wearable and Implantable Body Sensor Networks (BSN 2007)* (pp. 195–200). Berlin, Heidelberg: Springer Berlin Heidelberg. https://doi.org/10.1007/978-3-540-70994-7_34

Zhu, X. Q., & Law, S. S. (2006). Wavelet-based crack identification of bridge beam from operational deflection time history. *International Journal of Solids and Structures*, *43*(7–8), 2299–2317. <https://doi.org/10.1016/j.ijsolstr.2005.07.024>